

# Curcumin-loaded polymeric nanoparticles for neuroprotection in neonatal rats with hypoxic-ischemic encephalopathy

Andrea Joseph<sup>1</sup>, Thomas Wood<sup>2</sup>, Chih-Chung Chen<sup>1,†</sup>, Kylie Corry<sup>2</sup>, Jessica M. Snyder<sup>3</sup>, Sandra E. Juul<sup>2</sup>, Pratik Parikh<sup>2</sup>, and Elizabeth Nance<sup>1,4</sup> (✉)

<sup>1</sup> Department of Chemical Engineering, University of Washington, Seattle, WA 98195, USA

<sup>2</sup> Division of Neonatology, Department of Pediatrics, University of Washington, Seattle, WA 98195, USA

<sup>3</sup> Department of Comparative Medicine, University of Washington, Seattle, WA 98195, USA

<sup>4</sup> Department of Radiology, University of Washington, Seattle, WA 98195, USA

<sup>†</sup> Present address: Department of Bioengineering, University of Illinois at Urbana-Champaign, Urbana, Illinois 61801, USA

Received: 15 March 2018

Revised: 15 May 2018

Accepted: 18 May 2018

© Tsinghua University Press and Springer-Verlag GmbH Germany, part of Springer Nature 2018

## KEYWORDS

drug delivery,  
neuroprotection,  
brain penetrating,  
neonatal hypoxia-ischemia,  
curcumin,  
nanotherapeutics

## ABSTRACT

Hypoxic-ischemic encephalopathy is the leading cause of permanent brain injury in term newborns and currently has no cure. Inflammatory processes play a key role in the progression of this disease and may be amenable to a targeted pharmaceutical intervention. Curcumin is a dietary compound with potent anti-inflammatory, antioxidant, and antiapoptotic properties but is limited in therapeutic applications due to its low aqueous solubility, low bioavailability, and rapid first-pass hepatic metabolism. To address these limitations, loading curcumin into poly(lactic-co-glycolic acid)-poly(ethylene glycol) (PLGA-PEG) nanoparticles may increase relevant pharmacokinetic parameters and allow for effective drug delivery to the brain. Using the Vannucci model of unilateral hypoxic-ischemic brain injury in neonatal rats, we studied the *in vivo* effect of curcumin-loaded PLGA-PEG nanoparticles on brain uptake and diffusion of curcumin and on neuroprotection. The curcumin-loaded nanoparticles were able to overcome the impaired blood-brain barrier, diffuse effectively through the brain parenchyma, localize in regions of injury, and deliver a protective effect in the injured neonatal brain. The application of curcumin and PLGA-PEG nanoparticle-mediated delivery to a clinically relevant model of neonatal brain injury provides greater opportunities for clinical translation of targeted therapies for hypoxic-ischemic encephalopathy.

## 1 Introduction

Perinatal asphyxia (PA), where newborns suffer from

a lack of oxygen and blood flow to the brain, accounts for one of the highest numbers of disability-adjusted life years for any condition [1, 2]. PA can result in the

Address correspondence to eanance@uw.edu

development of hypoxic-ischemic (HI) brain injury and subsequent hypoxic-ischemic encephalopathy (HIE), which occurs in 1–3 per 1,000 live births in developed countries, and in as many as 26 per 1,000 live births in low-resource settings [3]. Without treatment, 20%–50% of affected infants die within the neonatal period, and up to 25% of survivors exhibit permanent neuropsychological handicaps including intellectual disability, cerebral palsy, epilepsy, or sensorineural hearing loss or vision loss, which carry a huge burden on society [4]. Currently, therapeutic hypothermia (TH) is the only clinically implemented treatment that has been shown to provide robust improvement in outcome among asphyxiated term newborn infants who develop moderate or severe HIE [5]. However, there still remains a 40%–50% risk of death or disability, motivating the search for additional interventions to reduce morbidity and mortality [6].

Neuroprotective agents such as xenon and erythropoietin (EPO) are being studied in clinical trials as adjuvants to TH [7, 8]. Nonetheless, no current potential therapy outperforms TH, even though TH may not always be appropriate or available, especially in the developing world [9]. Therefore, additional therapeutic interventions and delivery strategies still need to be explored. Preclinically, therapies with broad-spectrum activities including anti-inflammatory and antioxidant properties are thought to have a potential for pharmacological targeting of HI brain injury. Curcumin is a promising pharmacological agent because it has anti-inflammatory, antioxidant, and antiapoptotic effects and induces neurogenesis [10–12]. Curcumin is the active ingredient of turmeric, which has been traditionally consumed as a dietary component for centuries [13]. In pharmacological form, however, it has poor bioavailability due to its hydrophobic nature and rapid hepatic metabolism [14]. Incorporation of curcumin into a nanoparticle platform could alleviate current delivery limitations by increasing curcumin's solubility and improving curcumin's absorption, distribution, metabolism, and excretion profiles in the body.

Polymeric nanoparticles have been proposed as a means to improve drug delivery efficiency, reduce off-site effects, provide a sustained drug release, and

enable delivery of a diverse range of therapeutics [15]. Among the variety of polymers that can be used as delivery vehicles for the treatment of neurological disorders, some of the most promising are those made of poly(lactic-co-glycolic acid) (PLGA). For example, PLGA nanoparticles coated with the polysorbate 80 (P80) surfactant facilitate the delivery of a number of drugs that are unable to cross the blood–brain barrier (BBB) in free form [16]. PLGA nanoparticles have improved delivery of therapeutics to glioma [17], Alzheimer's disease [18, 19], glaucoma [20], traumatic brain injury [21], and other diseases of the central nervous system [22–24]. At a disease site, cell-specific delivery can be achieved by surface modifications on the PLGA polymer by means of targeting ligands, surfactants, or cell-penetrating peptides [25]. After crossing the BBB, the challenge of penetrating the brain parenchyma to diffuse long distances to reach diseased cells must also be overcome before those cells can be targeted. Dense poly(ethylene glycol) (PEG) surface coatings have been shown to improve polymeric nanoparticle diffusion in the brain parenchyma [26] in addition to increasing stability, solubility [27, 28], and circulation time of the nanoparticle system [29].

Curcumin nanoformulations have previously been shown to enhance therapeutic efficacy in a variety of animal models of neurological disorders [30], including reductions in edema, oxidative stress, inflammation, and apoptosis as well as improved behavioral outcomes [31–36]. Nonetheless, investigation of both curcumin and polymeric nanoparticles has not been carried out in the neonatal brain, with previous publications about adult models of brain injury, even though the newborn brain is uniquely vulnerable to brain injury [37, 38]. We therefore sought to test the neuroprotective effect of curcumin-loaded polymeric nanoparticles in the Vannucci rat model of neonatal HI brain injury.

## 2 Materials and methods

### 2.1 Materials

PLGA (50:50,  $M_w$  45 kDa) and PLGA (50:50,  $M_w$  45 kDa)-methoxy PEG (mPEG,  $M_w$  5 kDa) (PLGA-PEG) polymers were purchased from Akina

PolySciTech. Curcumin, Pluronic F127 (F127), and dimethyl sulfoxide (DMSO) were purchased from Sigma-Aldrich (St. Louis, MO, USA). High-performance liquid chromatography (HPLC)-grade formic acid, water, and acetonitrile were purchased from Fisher Scientific (St. Louis, MO, USA). All reagents and solvents were used as received. Cellulose ester dialysis membranes ( $M_w$  cutoff 300 kDa) were obtained from Spectrum Laboratories, Inc. (Rancho Dominguez, CA, USA).

## 2.2 Formulation of brain-penetrating curcumin-loaded nanoparticles

Curcumin-loaded nanoparticles were prepared by the nanoprecipitation method. PLGA-PEG or PLGA polymers were dissolved in acetone with 20% target curcumin loading. The polymer solution (organic phase) was then added dropwise into 25 mL of a 1% F127 surfactant solution, where nanoparticles formed spontaneously, and were stirred for 3 h at 700 rpm to remove the organic solvent. The organic solvent was further removed with rotary evaporation (Buchi Rotavapors, Buchi Corporation, New Castle, DE, USA) under reduced pressure (15 mbar) at 4 °C for 30 min. Nanoparticles were collected and washed twice by ultracentrifugation with deionized water at  $100,000 \times g$  for 25 min. Finally, the nanoparticles were resuspended in 1 mL of deionized water, or in sterile 1× phosphate buffered saline (PBS) for animal experiments. Nanoparticles were used immediately or were lyophilized with 20% (w/v) sucrose added as a cryoprotectant and stored at  $-80$  °C until needed. For fluorescently labeled nanoparticles, the same nanoparticle formulation procedure was carried out with PLGA and PLGA-PEG and conjugation of Alexa Fluor 555 (AF555) or Alexa Fluor 647 (AF647) dye was achieved by attachment to the free COOH group on the PLGA backbone, as described previously [26].

## 2.3 Particle size, polydispersity, zeta potential, and morphology

The particle size and polydispersity index (PDI) of curcumin-loaded PLGA-PEG (PLGA-PEG/curcumin) and curcumin-loaded PLGA (PLGA/curcumin) nanoparticles were measured by dynamic light scattering

(DLS), and the zeta potential ( $\zeta$ -potential) was determined using a zeta potential analyzer (NanoSizer Zeta Series, Malvern Instruments, Malvern, UK). Samples were diluted to appropriate concentrations to obtain accurate measurements in 10 mM sodium chloride (NaCl), pH 7.4, as described elsewhere [39].

## 2.4 Curcumin drug loading and encapsulation efficiency

Drug loading and encapsulation efficiency were determined by ultraviolet–visible light (UV–Vis) spectrometry as compared to a standard calibration curve of curcumin in DMSO. Each sample's absorbance at 430 nm was measured and adjusted by subtracting a blank of unloaded polymer nanoparticles' absorbance in DMSO. The weight of a polymer and drug was determined by lyophilizing the nanoparticle sample. Drug loading (DL) and drug encapsulation efficiency (DEE) are defined as follows

$$\% \text{ DL} = \frac{\text{Weight of drug encapsulated in NP}}{\text{Weight of polymer and drug in NP}} \quad (1)$$

$$\% \text{ DEE} = \frac{\text{Weight of drug encapsulated in NP}}{\text{Weight of drug used in formulation}} \quad (2)$$

## 2.5 An *in vitro* drug release profile

PLGA-PEG/curcumin and PLGA/curcumin nanoparticles were resuspended in 1 mL of 1× PBS. Each sample was evenly distributed to three dialysis tubes made of cellulose ester ( $M_w$  cutoff: 300 kDa, Spectrum Laboratories, Inc.). The membranes were submerged in 20 mL of 1× PBS containing 1% of P80 surfactant and placed on a shaker at 60 rpm and 37 °C. At designated time points, the membranes were transferred to fresh 20 mL of 1× PBS containing 1% of P80. In the supernatants collected at each time point, curcumin content was determined by UV–Vis compared to a calibration curve of curcumin in the 1× PBS 1% P80 solution. Percent curcumin released from the nanoparticles was defined as the curcumin amount released at a specific time point divided by the total curcumin encapsulated in the nanoparticles.

## 2.6 Animal experiments and an ethics statement

All animal procedures in this paper were approved

by the Institutional Animal Care and Use Committee of the University of Washington, Seattle, WA, USA. Time-mated pregnant female Sprague–Dawley rats (virus antibody-free CD® (SD) IGS, Charles River Laboratories, Raleigh, NC, USA) were purchased and arrived on estrous day 17 (E17). Dams were housed individually and allowed to acclimate to their environment for a minimum of 3 days prior to delivering. The day of birth was defined as postnatal day 0 (P0), postnatal day 1 as P1, and so forth. Litters containing both sexes were cross-fostered and culled to 12 animals early after birth. Before and after the experiment, each dam and her pups were housed under standard conditions with an automatic 12 h light/dark cycle, temperature range of 20–26 °C, and access to standard chow and autoclaved tap water *ad libitum*. The pups were checked for health daily.

## 2.7 A model of unilateral HI brain injury in neonatal rats

On P7, pups were separated from their dams, weighed and sexed, and randomized to experimental groups. Anesthesia with isoflurane (3% for induction, 1.5%–2.0% for maintenance) was given in 100% O<sub>2</sub> via a nose cone, under a dissecting microscope. The left carotid artery was identified and cauterized with fine-tip disposable cautery. The pups were maintained in a temperature-controlled water bath before and after undergoing unilateral ligation of the left carotid artery. After all the animals recovered from anesthesia, they were returned to the dams for a minimum of 30 min before placement in a hypoxic chamber in a temperature-controlled water bath. Once rectal temperature in a sentinel animal was stable at 36 °C for 5 min, the chamber was sealed, and 8% O<sub>2</sub> (92% N<sub>2</sub>) was administered at a rate of 2.5 L·min<sup>-1</sup>. Once the oxygen concentration within the chamber reached 8%, hypoxia was maintained for 135 min. For all experiments in this study, the temperature of pups was monitored during the nesting period and immediately after each dose of nanoparticles, saline, or a free drug.

## 2.8 PLGA-PEG nanoparticle uptake across the BBB

For nanoparticle localization and regional distribution,

HI pups ( $n = 6$ ) received 50 mg·kg<sup>-1</sup> AF647-PLGA-PEG particles intraperitoneally (i.p.) 30 min after hypoxia-ischemia. Pups were euthanized 24 h after HI injury, perfused, and the brain was removed and placed in formalin. Fluorescein isothiocyanate (FITC)-labeled dextran (3 kDa, Sigma) was injected 30 min after hypoxia-ischemia at a 7.5 g·kg<sup>-1</sup> dose to measure BBB extravasation [40]. For biodistribution, healthy pups ( $n = 6$ ) were injected with 150 mg·kg<sup>-1</sup> AF647-PLGA-PEG particles i.p. on P7, with HI pups ( $n = 10$ ) receiving the same dose 30 min after HI. The pups were euthanized 24 h after injection. Blood was collected before perfusion and organ extraction, and all organs were subsequently frozen at -80 °C. Serum was collected by centrifuging the blood sample at 2,000 ×  $g$  for 10 min and removing supernatant. Frozen brains were homogenized in PBS using a tissue homogenizer (Wilmad-LabGlass, NJ, USA) and centrifuged at 10,000 ×  $g$  for 10 min to remove cell debris. Nanoparticle concentrations in brain and serum samples were determined by comparison to a UV–Vis calibration curve of AF647-PLGA-PEG nanoparticles in PBS (excitation 625 nm and emission 665 nm). For each animal, the brain/serum ratio was calculated by first determining the concentration of PLGA-PEG in the brain in mg per mg of brain tissue and then dividing by the concentration of PLGA-PEG in serum in mg per mL of serum.

## 2.9 Drug administration

A total of 75 pups (42 males, 33 females) were randomized into four treatment groups: saline, free curcumin, blank PLGA-PEG nanoparticles, and curcumin-loaded PLGA-PEG nanoparticles. Curcumin dose was 10 mg·kg<sup>-1</sup> in the particle groups and 100 mg·kg<sup>-1</sup> in the free-drug group. In the free-drug group, curcumin was dissolved in DMSO and then diluted with twice the volume of saline. This amount of DMSO was necessary to maintain curcumin solubility, thus confirming the need for a nanoparticle delivery system for curcumin. Treatment was administered i.p. 30 min, 24 h, and 48 h after HI. Dosage and timing were based on previous research on the therapeutic window for pharmacological agents in the Vannucci model [41].

## 2.10 Brain slice preparation for live particle tracking experiments

Brain slices were prepared from P14 rat pups, as previously described [42]. Normal P14 rats were euthanized, and brains were quickly removed under sterile conditions. Fresh brain slices, 250–350  $\mu\text{m}$  thick, were prepared by means of a tissue chopper (McIlwain, Ted Pella, Inc, Redding, CA, USA) and a surgical dissecting scope. The slices were placed onto 30 mm cell culture membrane inserts with 0.4  $\mu\text{m}$  pore sized (Millipore, Billerica, MA, USA). The membranes were then placed in 35-mm plates containing 1 mL of a culture medium consisting of 50% of the minimal essential medium (Thermo Fisher Scientific, Waltham, MA, USA), 50% Hank's balanced salt solution (Thermo Fisher Scientific), 1% GlutaMAX (Thermo Fisher Scientific), and 1% of penicillin. The cultures were maintained at 37 °C, with constant humidity and 95% air and 5% CO<sub>2</sub>. Slices were used within 48 h for particle-tracking experiments.

## 2.11 Multiple particle tracking (MPT)

Fresh brain slices were prepared as described above and used for MPT analysis to evaluate the diffusive ability of PLGA/curcumin and PLGA-PEG/curcumin in the living brain [26, 43, 44]. The slices were transferred to 35 mm glass bottom imaging disks, and 2  $\mu\text{L}$  of AF555-labeled PLGA and PLGA-PEG particles were injected directly into brain tissue. Visualization of the nanoparticles was accomplished with the excitation and emission spectra specific to AF555 in two different general brain regions: the cortex and thalamus. Five 6.5 s videos were recorded per slice at 10 Hz and 40 $\times$  magnification via fluorescent microscopy with a CMOS camera (Hamamatsu Photonics Corporation, Bridgewater, NJ, USA) coupled with a confocal microscope (Nikon Instruments, Inc., Melville, NY, USA). Trajectories were calculated by means of the MOSAIC MPT ImageJ plugin, and geometrically averaged precision-weighted mean squared displacements (MSD) were calculated via a self-developed Python package. Effective diffusion coefficients for each particle type in each brain region were then extracted from MSD data, and average

diffusivity of the particle type was obtained from a weighted average of the two brain regions. At least 50 particles were tracked per sample, with  $n = 3$  independent brain samples per particle type.

## 2.12 Immunohistochemistry

PLGA-PEG uptake in the brain was evaluated as previously described [45, 46] by placing brains in a formalin-to-30% sucrose gradient and sectioning on a Leica cryostat into 30  $\mu\text{m}$  sections. For cell density and morphological qualitative evaluations, 10  $\mu\text{m}$  slices from a paraffinized brain were deparaffinized before staining. Primary antibodies for microglia (1:250 goat anti-Iba1, Abcam) and neurons (1:250 donkey anti-NeuN, Abcam) were prepared in 1 $\times$  PBS containing 0.01% of Triton X-100 (Sigma) and either normal donkey serum (Sigma) or normal goat serum (Sigma). Primary antibody solutions were added to tissue sections for 8–12 h incubation at 4 °C in a humidified chamber. The tissue slices were washed twice in 1 $\times$  PBS. Secondary antibodies were dissolved in 1 $\times$  PBS and added to tissue slices with incubation for 2 h. The slices were washed twice in 1 $\times$  PBS, then stained with 1:1,000 4',6-diamidino-2-phenylindole (DAPI) (Invitrogen). Slides were washed and dried for 30 min in the dark. Mounting medium (Dako, Agilent Technologies, Santa Clara, CA, USA) was added to each slide, and a glass coverslip was placed on top. Slides were stored at 4 °C (until imaged under an A1 confocal microscope (Nikon Instruments)) and at 20 °C for long-term storage.

## 2.13 Gross injury scoring and total area loss

At P10, the animals received an overdose of pentobarbital before transcatheter perfusion with 1 $\times$  PBS followed by 10% neutral-buffered formalin. Immediately following brain extraction, a photo of each whole brain was taken and subsequently analyzed by an individual who was blinded to group allocation. Gross brain injury in the hemisphere ipsilateral to ligation was assessed on a five-point ordinal scale (0–4) as follows: 0 = no injury, 1 = mild injury with < 25% lesion of the ipsilateral hemisphere, 2 = 25%–50% lesion, 3 = 51%–75% lesion, and 4 =  $\geq$  75%

injury, as previously described [47]. Whole brains were post-fixed in 10% neutral-buffered formalin for at least 48 h. Following the fixation, blocks of brain were obtained. Using external landmarks, brains were cut at approximately the level of the striatum (block 1) and at the level of the hippocampus and thalamus (block 2). The tissue samples were paraffin embedded, cut into 5- $\mu$ m sections, and stained with hematoxylin and eosin (H&E). Given some slide-to-slide variability in the first cohort of animals, four additional sections between the striatum and thalamus at 120  $\mu$ m intervals were prepared in the second cohort of animals. Slides were scanned in bright field with a 20 $\times$  objective using a Nanozoomer Digital Pathology slide scanner (Hamamatsu; Bridgewater, NJ, USA). Area loss analysis was performed as previously described [48]. Briefly, two 5  $\mu$ m sections from the slices best representing the cortex, hippocampus, basal ganglia, and thalamus were selected. Virtual slides were exported as 600 dpi images. The optical density and hemispheric area of each section were analyzed in the ImageJ software (National Institutes of Health, Bethesda, MD, USA) by another blinded individual. The average percentage area loss from the two sections (one at the level of the frontal cortex and the other at the midhippocampal level) was calculated using the following formula:  $[1 - (\text{ipsilateral area}/\text{contralateral area})] \times 100$ . Sections from two animals (one each in the blank PLGA-PEG nanoparticle (group) and PLGA-PEG/curcumin group) could not be analyzed for area loss because of damage to the tissue during processing.

#### 2.14 Histopathological evaluation

H&E-stained slides from saline ( $n = 17$ ); free curcumin ( $n = 18$ ); PLGA-PEG/curcumin ( $n = 20$ ); and blank PLGA-PEG nanoparticle ( $n = 20$ )-treated animals were evaluated by a board-certified veterinary pathologist blinded to the group assignment of rats. A previously reported nine-step scoring system for HIE [49] was employed, with modifications, to grade the following regions: cerebral cortex, striatum, thalamus, and hippocampus. There was some section-to-section variability, although all regions were present for

grading (or in severely affected animals were absent due to marked cystic necrosis) with the exception of one PLGA-PEG/curcumin-treated animal in which section 2 was further caudal and lacked a hippocampus. This animal had a severe disease elsewhere in the brain and was assigned the maximum score of 16. Lesions in the cortex, striatum, and thalamus were scored semiquantitatively using a 0–4 scale, where “0” was normal; “1” indicated scattered random neuronal necrosis or a small focal area (< 10%); “2” indicated columnar damage in the cortex involving layers II–IV or partly confluent or incomplete multifocal to coalescing neuronal cell necrosis or loss affecting 20%–30% of the region; “3” indicated large, confluent and complete injury affecting 40%–60% of the region (all layers of cortex); and “4” indicated markedly rarefied or cystic lesions with near complete loss of architecture (> 80% affected). Half scores were possible according to defined criteria (Table S1 in the Electronic Supplementary Material (ESM)). Scoring for the hippocampus was also performed on a 0–4 scale, with “1” indicating < 10% injury; “2” indicating 50% injury, “3” indicating 75% injury; and “4” indicating 100% injury (Table S1 in the ESM).

Scores from each region were summed to yield the final score, ranging from 0 to 16. For figures, the median score from each group was calculated and an animal representing that median score (or within 1 point of the median score) was used to show pathology in the various regions of the brain. Images of lesions captured from the digitally scanned slides were exported and plated in Adobe Photoshop Elements. Image brightness and contrast was adjusted using White Balance level and/or Auto Contrast manipulations were applied to the entire image. Original magnification and scale bars are stated.

#### 2.15 Statistical analysis

Pups carrying rectal probes were excluded from the final analysis, as the stress of carrying probes has previously been shown to have a neuroprotective effect [50]. Injury data are summarized as a median with 95% confidence interval (CI). Total area loss, gross injury, and global neuropathology scores were

compared by the two-tailed Wilcoxon–Mann–Whitney *U* test. Within the four treatment groups, three predetermined comparisons were performed for each outcome (PLGA-PEG/curcumin group compared to each group), and the Bonferroni correction was applied for multiple comparisons. Statistical analysis was performed in GraphPad version 7 (GraphPad Prism Software, San Diego, CA, USA). Data with a *p* value < 0.05 were considered statistically significant.

### 3 Results

#### 3.1 Preparation and characterization of curcumin-loaded nanoparticles

Brain-penetrating curcumin-loaded nanoparticles were synthesized using the PLGA polymer or PLGA-PEG diblock copolymer via the nanoprecipitation method. After formulation of curcumin-loaded

nanoparticles, nanoparticle hydrodynamic size, PDI, and zeta-potential were determined by DLS and Zetasizer, and curcumin loading and efficiency were measured by UV–Vis spectroscopy (Table 1). PLGA/curcumin nanoparticles had a size, zeta potential, and PDI of 58.8 nm,  $-5.0$  mV, and 0.2, respectively, whereas PLGA-PEG/curcumin nanoparticles had similar physicochemical characteristics of 61.1 nm,  $-2.7$  mV, and 0.1. The PLGA-PEG/curcumin nanoparticles achieved marginally higher curcumin loading (6.00%) than PLGA/curcumin nanoparticles (5.27%). Drug release assays showed burst release phenomena in both PLGA and PLGA-PEG particles, with a 40% and 49% curcumin release, respectively, in the first 4 h, followed by a sustained phase releasing up to 59% or 99% curcumin in the next 4 days (Fig. 1(a)). Scanning electron microscopy (SEM) imaging showed similar spherical morphology for blank PLGA-PEG and PLGA-PEG/curcumin nanoparticles (Fig. 1(b)).

**Table 1** Physicochemical properties of PLGA and PLGA-PEG nanoparticles loaded with curcumin. PLGA and PLGA-PEG nanoparticles loaded with curcumin were characterized in terms of hydrodynamic diameter, mean surface charge ( $\zeta$ -potential), and the polydispersity index by dynamic light scattering at 37 °C and pH 7.2 in 10 mM NaCl. DL and DEE were measured by UV–Vis spectroscopy. All values are reported as mean  $\pm$  standard error of the mean (S.E.M.)

Particle type	PEG % (w/w)	Mean size $\pm$ SEM (nm)	Mean ZP $\pm$ SEM (mV)	Mean PDI $\pm$ SEM	DL $\pm$ SEM (%)	DEE $\pm$ SEM (%)
PLGA45k (50:50)/curcumin	0	58.8 $\pm$ 2.0	$-5.0 \pm 0.2$	0.2 $\pm$ 0.01	5.3 $\pm$ 0.1	46.0 $\pm$ 21.0
mPEG5k-PLGA45k (50:50)/curcumin	10	61.1 $\pm$ 0.8	$-2.7 \pm 0.1$	0.1 $\pm$ 0.05	6.0 $\pm$ 0.5	27.3 $\pm$ 2.6

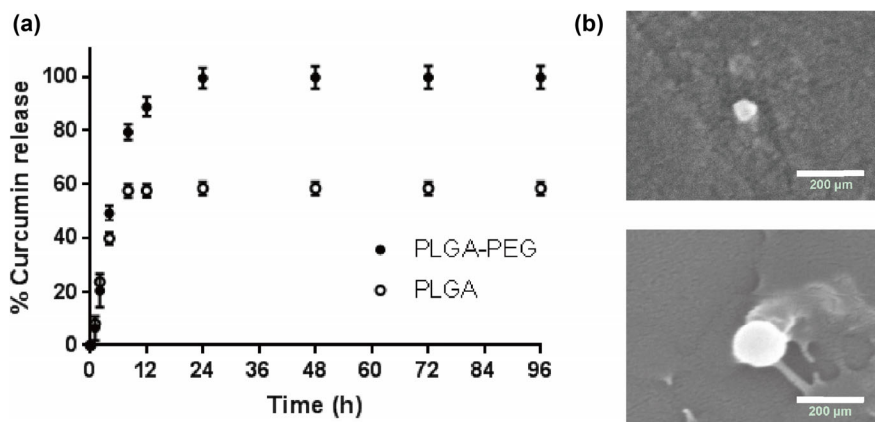


**Figure 1** Curcumin release kinetics from PLGA and PLGA-PEG nanoparticles. PLGA and PLGA-PEG nanoparticles loaded with curcumin were incubated in 1 $\times$  PBS with 1% P80 at 37 °C, and samples were collected during 96 h. (a) Approximately 80% of curcumin was released from PLGA-PEG nanoparticles within 8 h; 41.19% more curcumin was released from PLGA-PEG nanoparticles compared with PLGA nanoparticles within 96 h. (b) SEM images show that curcumin-loaded PLGA-PEG and blank PLGA-PEG nanoparticles are spherical in shape.

### 3.2 PLGA-PEG nanoparticles can diffuse in the brain parenchyma

AF555-PLGA-PEG nanoparticle diffusivity was determined to ensure that the particles are capable of moving within the brain microenvironment (Fig. 2) to reach target cells, upon reaching the brain after systemic administration. Diffusion analysis revealed that PLGA-PEG nanoparticles had a diffusivity of  $0.1 \mu\text{m}^2\cdot\text{s}^{-1}$  in the cortex (Fig. 2(a)) and  $0.085 \mu\text{m}^2\cdot\text{s}^{-1}$  in the thalamus (Fig. 2(b)). This was a 10-fold increase in diffusivity over PLGA particles in the cortex ( $0.01 \mu\text{m}^2\cdot\text{s}^{-1}$ ), and a 20-fold increase in diffusivity in the thalamus ( $0.004 \mu\text{m}^2\cdot\text{s}^{-1}$ ). Overall, PLGA-PEG nanoparticles had on average a 14-fold higher diffusive ability, 1.1-fold greater drug loading, and a 35% increase in a drug release as compared to PLGA nanoparticles. Therefore, PLGA-PEG nanoparticles were chosen for evaluation of the therapeutic effect *in vivo* in the rat model of neonatal HI brain injury.

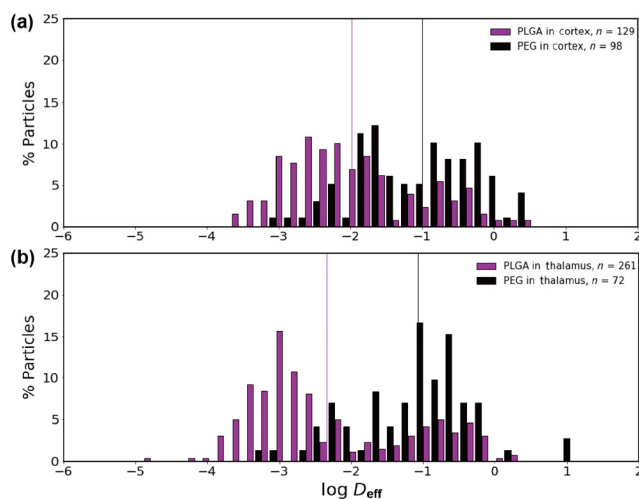


**Figure 2** Nanoparticle diffusion within the brain parenchyma. P14 organotypic brain slices were treated with AF555-labeled PLGA and PLGA-PEG nanoparticles. MPT videos were recorded, and individual particles tracked. (a) A log plot of effective diffusion coefficients of PLGA ( $n = 129$ ) and PLGA-PEG nanoparticles ( $n = 98$  particles) in the cortex of P14 organotypic brain tissue slices. The average  $D_{\text{eff}}$  in the cortex is  $0.01 \mu\text{m}^2\cdot\text{s}^{-1}$  for PLGA nanoparticles and  $0.1 \mu\text{m}^2\cdot\text{s}^{-1}$  for PLGA-PEG nanoparticles. (b) A log plot of effective diffusion coefficients of PLGA ( $n = 261$  particles) and PLGA-PEG nanoparticles ( $n = 72$  particles) in the thalamus of P14 organotypic brain tissue slices. The average  $D_{\text{eff}}$  in the thalamus is  $0.004 \mu\text{m}^2\cdot\text{s}^{-1}$  for PLGA nanoparticles and  $0.085 \mu\text{m}^2\cdot\text{s}^{-1}$  for PLGA-PEG nanoparticles. Data represent means of at least three experiments in three brain slices.

### 3.3 PLGA-PEG nanoparticles can overcome the BBB and extravasate into the parenchyma of the HI brain

AF647-PLGA-PEG nanoparticles accumulated in the hippocampus, dentate gyrus, and thalamus in the ipsilateral hemisphere of the HI brain (Fig. 3(a)). PLGA-PEG nanoparticle localization in the brain was detected in the ipsilateral hemisphere in regions with dextran-FITC extravasation (Fig. S1 in the ESM), although there was no apparent colocalization in Iba1<sup>+</sup> amoeboid microglial cells (Fig. 3(b)) in the CA1 region of the ipsilateral hippocampus. Quantification of AF647-PLGA-PEG nanoparticles in healthy and injured pups (Fig. S2 in the ESM) showed 3-fold higher nanoparticle accumulation in the injured brain (average brain/serum ratio 0.014) compared to the healthy brain (average brain/serum ratio 0.005;  $p = 0.0037$ ). PLGA-PEG extravasation into the brain parenchyma indicates that the nanoparticle can leverage the impaired BBB to deliver therapeutic payload within

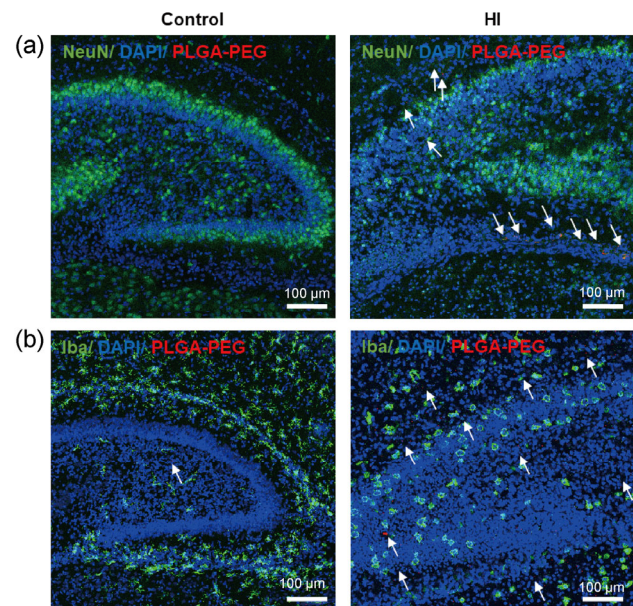


**Figure 3** Nanoparticle uptake in regions of injury in the HI brain. AF647-labeled PLGA-PEG nanoparticles ( $50 \text{ mg}\cdot\text{kg}^{-1}$ , red) were administered *i.p.* to P7 pups 30 min after HI. The pups were euthanized 24 h after hypoxia-ischemia and perfused. (a) PLGA-PEG localization near NeuN<sup>+</sup> neurons (green) is visible in the ipsilateral (injured, right-hand image) hemisphere of HI pups. There is no visible uptake near neurons in healthy pups (left-hand image). (b) PLGA-PEG localization near Iba<sup>+</sup> microglia (green) is also present in the ipsilateral hemisphere in HI pups and absent in uninjured pups. Blue: DAPI staining of cell nuclei.

proximity of cells involved in ongoing injurious pathways.

### 3.4 Curcumin-loaded PLGA-PEG nanoparticle treatment reduces global injury in the Vannucci model

Following i.p. injection of blank PLGA-PEG (250 mg·kg<sup>-1</sup>), PLGA-PEG/curcumin (10 mg·kg<sup>-1</sup> curcumin, 250 mg·kg<sup>-1</sup> PLGA-PEG), free curcumin (100 mg·kg<sup>-1</sup>), or saline (10 mL·kg<sup>-1</sup>) into HI pups at 30 min, 24 h, and 48 h after hypoxia-ischemia, gross injury scores decreased significantly from a median (95% CI) of 3 (3–4;  $p = 0.006$ ), 3.5 (1–4;  $p = 0.03$ ), and 4 (3–4;  $p = 0.003$ ) in the saline, free curcumin, and blank PLGA-PEG groups, respectively, compared to a median of 0 (0–3) in the PLGA-PEG/curcumin group. Representative median brains are shown in Fig. S3 in the ESM. Total area loss showed similar results (Fig. 4(b)). The median (95% CI) hemispheric area loss of the left side was 37.2% (27.9%–51.4%), 37.8% (20.2%–44.2%), 35.4% (6.0%–44.4%), and 12.3% (3.6%–26.8%), in the saline, free curcumin, blank PLGA-PEG, and PLGA-

PEG/curcumin groups, respectively. Area loss was significantly lower in the PLGA-PEG/curcumin compared to the saline ( $p = 0.006$ ) and free curcumin groups ( $p = 0.04$ ). An initial trend ( $p = 0.07$ ) towards a significant difference in area loss between the PLGA-PEG/curcumin and blank PLGA-PEG nanoparticle groups did not remain after adjustment for multiple comparisons.

### 3.5 Curcumin-loaded PLGA-PEG nanoparticle treatment does not result in region-specific neuroprotection

Marked variation in a region-specific response to treatment was seen in histopathological analysis. A plot of region-specific pathology scores by group is presented in Fig. 5. H&E images showing representative pathology in the different areas assessed are shown in Fig. 6. The median (95% CI) total pathological score (maximum 16) was 12.5 (10–14.5), 12.3 (9–14.5), and 13.3 (8.5–15) in the saline, free curcumin, and blank PLGA-PEG particle groups, respectively, and 6.5 (2.5–15.0) in the PLGA-PEG/curcumin nanoparticle

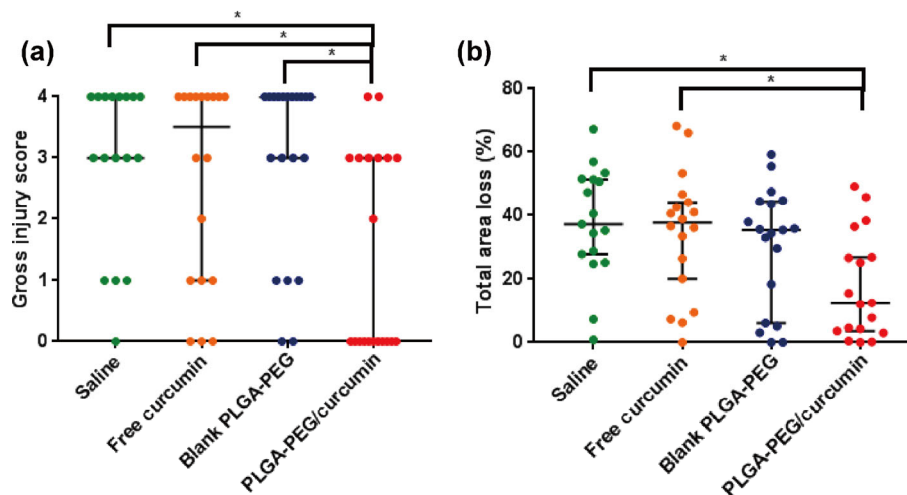


**Figure 4** PLGA-PEG/curcumin effects on global brain injury and percent area loss in the HI brain. HI pups were treated 30 min, 24 h, and 48 h after HI injury with saline, free curcumin, blank nanoparticles, or PLGA-PEG/curcumin. The pups were euthanized on P10, 72 h after HI injury. All analyses were performed in a blinded manner. (a) Gross injury was assessed on a 0 (least injured) to 4 (most injured) scale for all groups. Median (95% CI) scores were as follows: saline: 3 (3–4;  $n = 16$ ), free curcumin: 3.5 (1–4;  $n = 19$ ), blank PLGA-PEG particles: 4 (3–4;  $n = 20$ ); PLGA-PEG/curcumin: 0 (0–3;  $n = 20$ ). Significant differences were seen between PLGA-PEG/curcumin and saline ( $p = 0.006$ ), free curcumin ( $p = 0.03$ ), or blank PLGA-PEG ( $p = 0.003$ ). (b) Total area of loss was calculated by assessing the percent area of tissue lost in the ipsilateral hemisphere, normalized to the contralateral hemisphere. Median (95% CI) area losses were as follows: saline: 37.2% (27.9%–51.4%;  $n = 16$ ), free curcumin: 37.8% (20.2%–44.2%;  $n = 19$ ), blank PLGA-PEG particles: 35.4% (6.0%–44.4%;  $n = 18$ ), and PLGA-PEG/curcumin: 12.3% (3.6%–26.8%;  $n = 19$ ). Significant differences were seen between PLGA-PEG/curcumin and saline ( $p = 0.006$ ) or free curcumin ( $p = 0.04$ ) groups. \*A significant difference as compared to all other groups. Group differences were evaluated by the two-tailed Wilcoxon–Mann–Whitney  $U$  test, with Bonferroni’s correction for multiple comparisons.

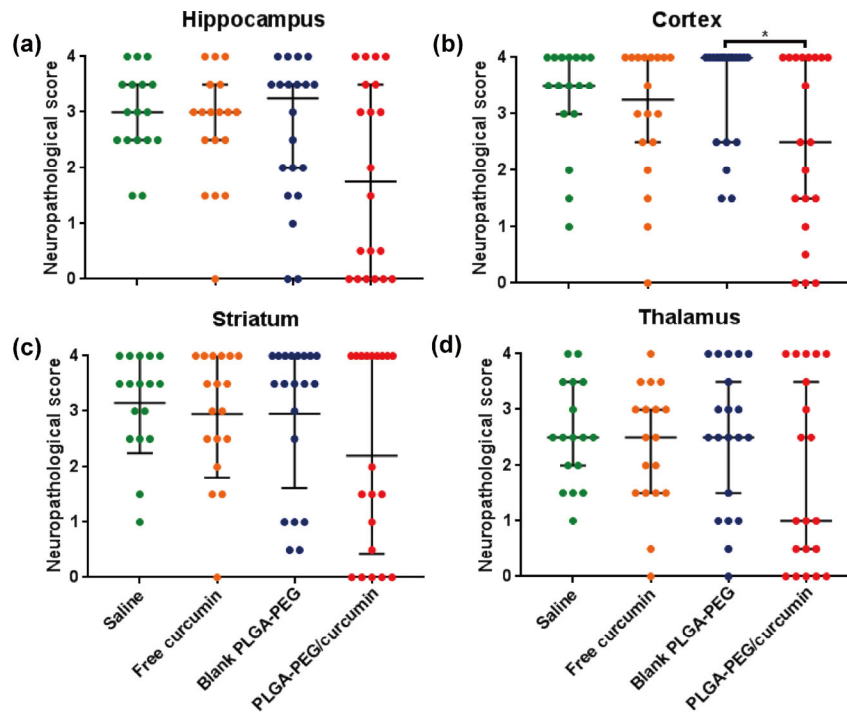


**Figure 5** Neuropathology after PLGA-PEG/curcumin treatment of HI pups. These pups were treated 30 min, 24 h, and 48 h after unilateral HI injury with saline, free curcumin, blank PLGA-PEG nanoparticles, or PLGA-PEG/curcumin nanoparticles. The pups were euthanized on P10, 72 h after HI injury. Neuropathological analyses were performed in a blinded manner. Four regions (hippocampus, cortex, striatum, and thalamus) on the unilateral side were scored on a 9-point scale between 0 (least injured) and 4 (most injured). Though the median score was the lowest in the PLGA-PEG/curcumin group for all measures, a significant difference was seen only in the cortex between blank PLGA-PEG and PLGA-PEG/curcumin ( $p = 0.0249$ ). Group differences were evaluated using the two-tailed Wilcoxon–Mann–Whitney  $U$  test, with Bonferroni’s correction for multiple comparisons.

group. A similar pattern of decreased median pathology score in the PLGA-PEG/curcumin group was seen in the cortex (Fig. 5(a)), thalamus (Fig. 5(b)), hippocampus (Fig. 5(c)), and striatum (Fig. 5(d)); however, none of these differences were statistically significant. A summary of pathology scores, as well as gross injury and area loss analysis across all groups is shown in Table 2.

Blank-PLGA-PEG-treated, free-curcumin-treated, and saline-treated animals tended to have more severe, extensive necrosis of the anterior cortex and middle cortex (Fig. 6), often with rarefaction of the neuropil. In the striatum, hippocampus, and thalamus, we observed moderate-to-marked multifocal to coalescing neuronal necrosis and cell loss. In contrast, lesions in more PLGA-PEG/curcumin-treated than blank-PLGA-PEG-treated animals were more often characterized by mild to moderate columnar necrosis in the cerebral cortex, and mild, patchy neuronal necrosis in the striatum, thalamus, and hippocampus

(Fig. 6). Furthermore, more PLGA-PEG/curcumin treated animals had minimal to no neuropathology, with eight animals receiving a total neuropathology score lower than 4 (three animals with a score of 0; two animals with a score of 2; and one animal each with a score of 2.5, 3, or 3.5). In contrast, only one animal in each of the blank PLGA-PEG and free curcumin groups scored less than 4, and no saline-treated animals received a score lower than 6. Severe injury characterized by variably severe (but generally minimal to mild) involvement of the contralateral hemisphere was observed in all treatment groups (three saline-treated animals; one free-curcumin-treated animal; six blank-PLGA-PEG-treated animals; and four PLGA-PEG/curcumin-treated animals).

### 3.6 Microglia show altered morphology following PLGA-PEG/curcumin nanoparticle treatment

We observed an increase in microglial numbers (Iba<sup>+</sup> cells), and a change in microglial morphology,

**Table 2** Outcome measures after treatment in neonatal HI rats. The rats were subjected to hypoxia-ischemia on P7, and treatments (saline, free curcumin, blank PLGA-PEG, and PLGA-PEG/curcumin) were administered at 30 min, 24 h, and 48 h after HI. All outcome measures were assessed 72 h after HI injury. For each outcome measure, median (95% CI) gross injury, area loss, and regional and total pathology score across the four treatment groups is provided. \*A significant difference in comparison with all other groups. #A significant difference as compared to saline and free curcumin groups. Group differences were evaluated by the two-tailed Wilcoxon–Mann–Whitney *U* test, with Bonferroni’s correction for multiple comparisons

	Group (median; 95% CI)				
	Saline	Free curcumin	Blank PLGA-PEG	PLGA-PEG/curcumin	
Gross injury	3 (3–4)	3.5 (1–4)	4 (3–4)	0 (0–3)*	
Area loss (%)	37.2 (27.9–51.4)	37.8 (20.2–44.2)	35.4 (6.0–44.4)	12.3 (3.6–26.8)#	
Pathology scores:					
Injury assessment	Cortex	3.5 (3.0–4.0)	3.3 (2.5–4.0)	4.0 (2.5–4.0)	2.5 (1.5–4.0)
	Hippocampus	3 (2.5–3.5)	3 (2.5–3.5)	3.3 (2.0–3.5)	1.8 (0.0–3.5)
	Striatum	3.5 (2.5–4.0)	3.3 (2.5–4.0)	3.5 (2.5–4.0)	1.8 (0.5–4.0)
	Thalamus	2.5 (2.0–3.5)	2.5 (1.5–3.0)	2.5 (1.5–3.5)	1 (0.5–3.5)
	Total pathology score	12.5 (10.0–14.5)	12.3 (9.0–14.5)	13.3 (8.5–15.0)	6.5 (2.5–15.0)

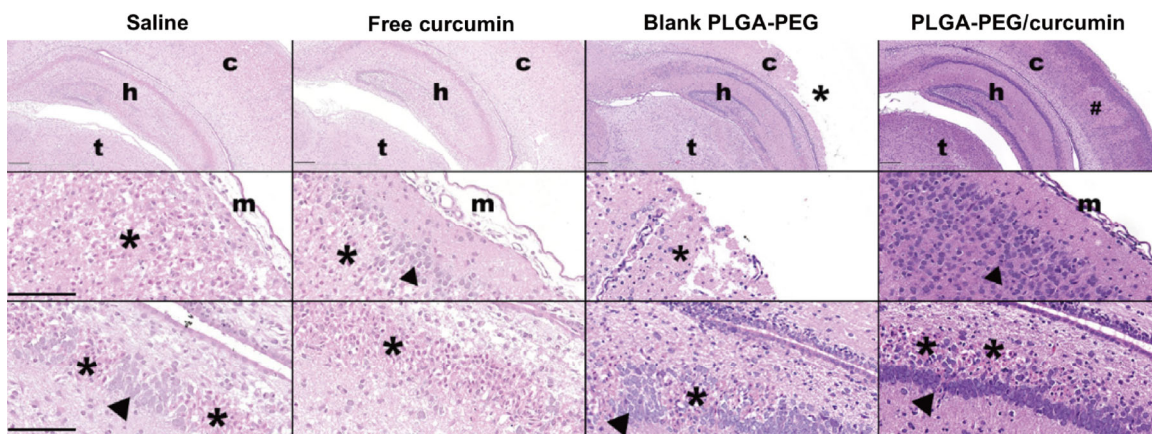


**Figure 6** Representative histological images of PLGA-PEG/curcumin-treated pups. Left column: a saline-treated animal; left center: a free-curcumin-treated animal; right center: a blank PLGA-PEG-treated animal; right column: a PLGA-PEG/curcumin-treated animal. Animals within 1 point of the treatment group median are pictured. Top row: Lower-magnification view of the hippocampus (h) and cerebral cortex (c) at the level of the thalamus (t). In the saline-, free-curcumin-, and blank PLGA-PEG-treated animals, there is moderate to regionally marked disorganization and neuronal death in the cortex with a portion of ischemic cortex missing (\*) in the blank PLGA-PEG-treated animal. In the PLGA-PEG/curcumin-treated animal, there is mild multifocal columnar neuronal cell necrosis and loss (#). Scale bar = 0.25 mm. Middle row: Higher-magnification view of neuronal cell death and loss with disorganization of the cortex (\*). Normal neurons are indicated by the triangle. M = meninges. Scale bar = 100  $\mu$ m. Bottom row: hippocampus (CA1 and CA2) with regionally extensive neuronal necrosis and loss (\*). Normal neurons are indicated by the triangle. Scale bar = 100 microns.

in the brains of the saline, free curcumin, and blank nanoparticle treatment groups 72 h after HI injury (Fig. 7(a)). Microglial morphology was more amoeboid in shape in the dentate gyrus, CA1, and subcortex of the ipsilateral hemisphere in the saline, free curcumin, and blank nanoparticle groups, with no differences

in morphology seen between them. On the other hand, PLGA-PEG/curcumin-treated animals showed reduced microglial numbers, and fewer amoeboid morphological features. In particular, in the CA1 region in the PLGA-PEG/curcumin-treated pups, microglia were more elongated. A few cell processes were also

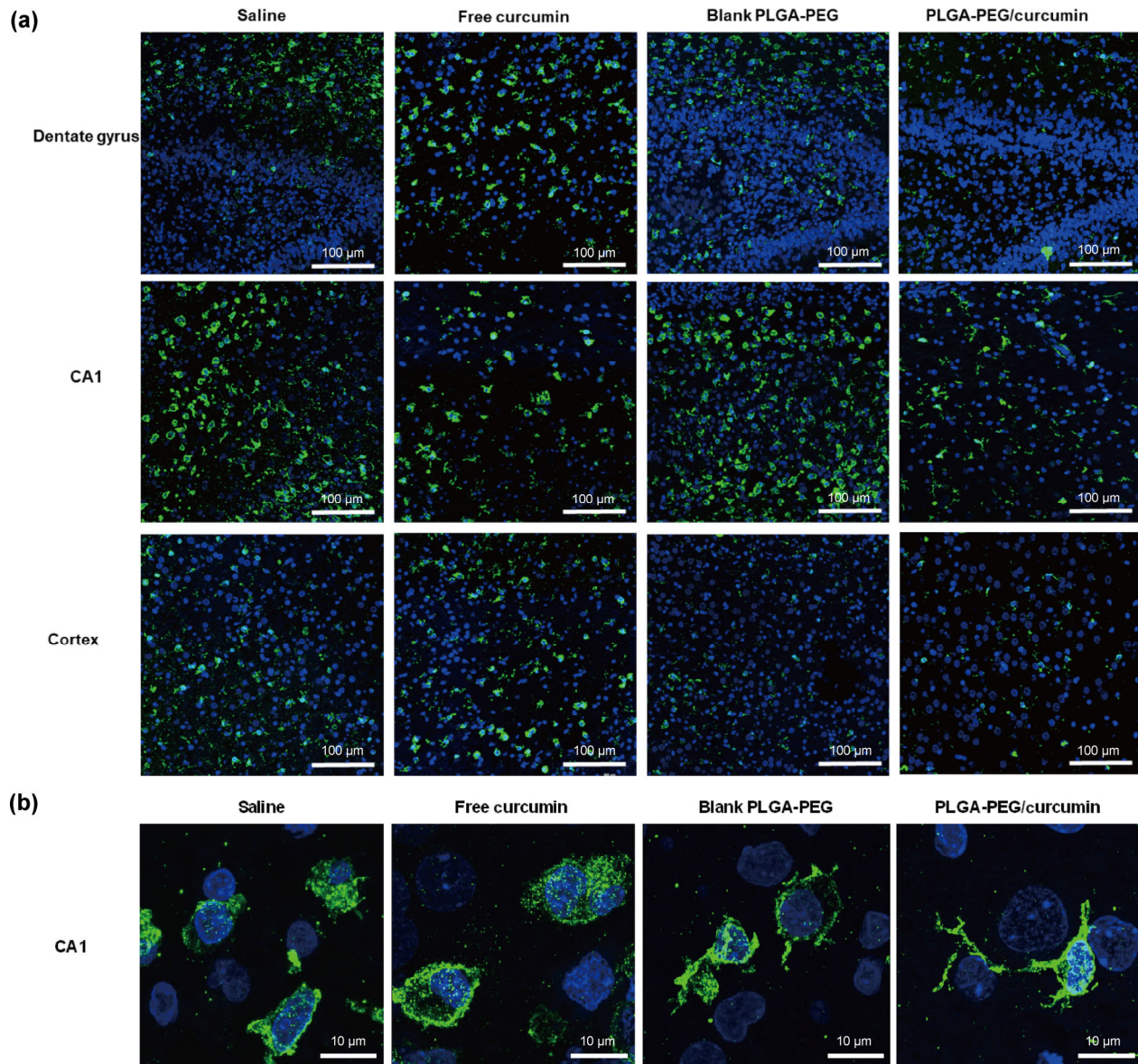


**Figure 7** Neuronal density after hypoxia-ischemia and PLGA-PEG/curcumin treatment. (a) The presence of Iba1<sup>+</sup> microglia (green) was evaluated for all treatment groups in regions of injury in the HI brain, including the cortex, CA1, and dentate gyrus. The microglia number is greater in all control groups (saline, free curcumin, and blank PLGA-PEG), and morphology shifted to an amoeboid phenotype. PLGA-PEG/curcumin-treated microglia appear to be fewer in number and (b) partially ramified. Blue: DAPI staining of cell nuclei.

present, potentially indicating a return to a more normal ramified state (Fig. 7(b)). The morphological changes in microglia were confined to regions of neuronal injury, which included the CA1 region of the hippocampus, subcortex, and the caudate putamen.

#### 4 Discussion

PA and resulting HIE are leading causes of morbidity and mortality around the time of birth [5]. Although

TH is currently the only validated treatment of HIE, it is not universally neuroprotective. Unfortunately, 40%–50% of treated infants with moderate and severe HIE will still die or have significant neurological disability [51]. Because the development of TH into a neuroprotective strategy for neonates was based on preclinical research in a number of animal models, there is scope to use these same models to develop pharmacological interventions as an adjuvant to TH. For instance, Juul et al. demonstrated the neuroprotective

effects of recombinant human EPO in the Vannucci rat model; this effect was more recently translated to clinical trials on term infants and extremely low-gestation neonates [52]. Analogously to the pleiotropic neuroprotective effects of both TH and EPO, the present study suggests that curcumin affects the progression of brain injury through multiple pathways, ultimately delivering a neuroprotective effect, which is enhanced by the PLGA-PEG nanoparticles.

Significant neuroprotection was seen in the PLGA-PEG/curcumin treatment group compared to all control groups (saline, free curcumin, and blank nanoparticles) after gross brain injury scoring. Hemispheric area loss also showed significant neuroprotection ( $p < 0.05$ ) in the PLGA-PEG/curcumin treatment group compared to all control groups. Nonetheless, after adjustment for multiple comparisons, no significant difference was seen between the PLGA-PEG/curcumin and blank PLGA-PEG groups. This result might be due to a therapeutic effect of the PLGA-PEG polymer itself, because others have shown that PEG can suppress reactive oxygen species production after injury by limiting superoxide generation [53]. Despite the significant decrease in global injury measures (gross injury and area loss), no significant decreases in region-specific or total formal pathology score were seen in the PLGA-PEG/curcumin group. This finding may be due to a lack of resolution in the gross injury score, or the fact that the formal pathology scoring system includes the subcortical structures not seen during gross injury score.

The difference in efficacy between measures may also give clues to where the PLGA-PEG/curcumin is exerting its effects. Both area loss and pathology scoring are concentrated in the areas at the center of the unilateral infarct that are most susceptible to injury [48, 54]. By comparison, gross injury scoring includes the total infarct area, including the penumbral region [55]. The dramatic decrease in the gross injury score suggests that PLGA-PEG/curcumin may be most beneficial at the penumbra, and that it is neuroprotective for cells that are less severely affected by the insult. This notion is also supported by the fact that the median pathology score (both total and region-specific) decreased in the PLGA-PEG/curcumin group, but the upper bounds of the

95% CI did not, suggesting that any neuroprotective effect of PLGA-PEG/curcumin nanoparticles was particularly absent in the most severely-injured animals. This is not an uncommon finding in the field, with TH and other therapies, including xenon, potentially unable to reverse injury once it is beyond certain severity [54, 56]. In fact, comparing the pathology scores seen in our current study to similar data in previous work suggests that the injury produced in this model was relatively severe [48], with many animals experiencing complete structural loss of the ipsilateral hemisphere, with involvement of the contralateral side [57]. Certain aspects of the response to injury may also prevent optimal penetration of the particles and delivery of the therapeutic agent. Edema formation in the most severely affected animals may reduce penetration of the nanoparticles into the core of the infarct. Though nanoparticle penetration into the region of injury was seen, and a therapeutic effect was achieved according to gross injury analysis, uniform distribution of a therapeutic agent from the penumbra to the core is necessary to achieve maximal efficacy [58, 59]. Coadministration of PLGA-PEG/curcumin with therapies that reduce edema formation, such as TH, may augment the effects of the nanoparticles, and this combination will be a focus of future work.

Polymeric nanoparticle systems have been widely used to improve biodistribution and bioavailability of therapeutics. Nanoparticles coated with special surfactants, such as P80 [60, 61], Poloxamer 188 (also referred to as Pluronic F68) [60, 62], or with chitosan [64] have also been shown to target the brain after systemic injection, even with an intact BBB, by adhering to and entering endothelial cells of the BBB. Nonetheless, the nanoparticles coated with P80 or F68 in these experiments possessed surface charges in the  $-20$  to  $-40$  mV range, and the chitosan-coated particles were 260 nm in diameter, thereby making it unlikely that these specific particles were capable of diffusing into the brain beyond the BBB endothelium [26, 43]. The curcumin-loaded particles evaluated in the present study were  $\sim 60$  nm in diameter and had a near-neutral surface charge: both characteristics that enhance penetration of nanotherapeutics within the brain parenchyma. Additionally, PEG copolymerization

to PLGA imparts steric stability for improved nanoparticle bioavailability after systemic administration [64, 65]. The PLGA-PEG nanoparticles used in this study demonstrated a 10-fold higher diffusive ability in the cortex and 20-fold higher diffusivity in the thalamus as compared to the PLGA formulation. This phenomenon is likely due to the “stealth” nature of PEG-coated particles that limits interaction with cells and proteins in the cerebral extracellular space [44]. The increased diffusive ability is noteworthy because it allows the nanoparticle and curcumin payload to achieve greater dispersion in the brain, a property that correlates with the efficacy of many therapeutics [15, 66, 67].

A greater drug release from curcumin-loaded PLGA nanoparticles was achieved by modifying surface functionality with the PEG polymer. PEG, as an amphiphilic polymer, can increase the surface area of a nanoparticle and therefore expand the fraction of curcumin that is adsorbed onto, or weakly bound to, the nanoparticle surface [68]. The early burst release phase is therefore dominated by a drug release from near the nanoparticle surface, as seen in the PLGA-PEG/curcumin formulation, which yielded a greater burst release (40% from PLGA and 49% from PLGA-PEG within 4 h) and greater controlled release during 96 h (59% vs. 99%) as compared to the PLGA/curcumin formulation [69].

After being delivered to the injured brain, curcumin can act on HI injury through multiple pathways. Others have demonstrated therapeutic properties of curcumin, including both antioxidant [70, 71] and anti-inflammatory [72, 73] effects. Curcumin's anti-inflammatory effects are due to inhibition of nuclear factor kappa B (NF- $\kappa$ B) signaling, thereby leading to downregulation of proinflammatory cytokines and enzymes [73, 74]. *In vitro* and *in vivo* studies indicate that curcumin's antioxidant effects arise from direct scavenging via the phenolic structure, as well as modulation of nuclear factor (erythroid-derived 2)-like 2 (Nrf2) pathway [71]. Besides, curcumin inhibits activation of the NMDA receptor for glutamate, which is central to the initiation of the excito-oxidative cascade that results in necrosis and apoptosis from mitochondrial damage after HI injury [75]. Finally, curcumin induces neurogenesis by modulating

the canonical Wnt- $\beta$ -catenin pathway, leading to reversal of cognitive deficits in models of Alzheimer's disease [76].

PLGA-PEG nanoparticle uptake in the injured brain was observed within 24 h in the regions of injury. Nanoparticle uptake and extravasation into regions of injury and proximity to amoeboid microglia and injured neurons are important because both cell types are implicated in the progression of HI brain injury. During inflammation, microglia proliferate, with a shift in phenotype from ramified healthy surveying microglia to a spectrum of more amoeboid “activated” microglia [77–79]. After 72 h of therapy, microglia were fewer in number in the PLGA-PEG/curcumin group, with a more ramified morphology, compared to the control groups. This finding suggests that PLGA-PEG/curcumin is capable of selectively altering microglial function in areas of injury, and this effect may reduce the long-term inflammatory responses to hypoxia-ischemia that contribute to the secondary and tertiary phases of injury [80]. Nonetheless, longer-term outcomes may be needed to discriminate the benefit seen in the changing microglial phenotype in the PLGA-PEG/curcumin group.

The brain uptake and region-specific localization of the polymeric nanoparticle platform can be important for targeted delivery, especially if toxicity of a drug is of concern. It should be emphasized that minimal or no nanoparticle uptake is seen in regions of healthy tissue; this effect will reduce off-site toxicity and minimize any long-term unwanted effects. Instead, the PLGA-PEG/curcumin nanoparticles leverage both BBB breakdown in regions of injury and nanoparticle stealth properties to get distributed specifically within the injured brain parenchyma. The ability of the PLGA-PEG/curcumin particles to deliver a broad-acting therapeutic to injured cells for neuroprotection, without associated toxicity, highlights the advantages of the nanoparticle platform for targeted delivery.

Limitations to this study include the relatively early (72 h) assessment of injury, and the absence of behavioral outcomes. For instance, compared to previous work that assessed area loss at P14, one week after injury [48, 54], area loss at P10 may underestimate final tissue loss due to a shorter time

period for the injury to evolve. Future studies with longer follow-up after the injury may allow for greater resolution in terms of comparing injury severity among different treatment groups. Additionally, due to the limited solubility of curcumin, DMSO was needed in addition to PBS as a delivery vehicle for the free-curcumin treatment. Other studies involving DMSO at concentrations ranging from 0.1% (v/v) to 100% to deliver curcumin in cell cultures have revealed no significant cytotoxicity [81–84]. DMSO has also been employed to deliver melatonin in the neonatal hypoxia-ischemia model, and no significant neurotoxic effect was found in DMSO and PBS treatment groups [85]. When an effect has been detected with DMSO at concentrations similar to the ones used to deliver curcumin in adult brain injury models, it has instead tended to cause neuroprotection rather than neurotoxicity [86]. The conflicting literature data and the need for DMSO to solubilize curcumin further justify the use of the nanoparticle-based delivery platform. Lastly, our experiment was not designed to evaluate sex-based differences. Significant changes in outcome based on sex have been observed both in preclinical models and in clinical settings, and males and females may have different requirements for interventions that modulate oxidative stress [87–92]. To further support the use of curcumin-loaded nanoparticles as a pharmaceutical intervention in perinatal brain injury, PLGA-PEG/curcumin must be compared as a competitor to treatments like EPO and N-acetyl cysteine (NAC), which have shown efficacy in injury models comparable to the Vannucci model [41, 93]. The increased efficacy of the PLGA-PEG/curcumin particles over free curcumin also supports the idea that other potential agents besides curcumin that undergo delivery or encounter pharmacokinetic barriers to neuroprotection could be loaded into similar particles. Nevertheless, this is the first study that proves the neuroprotective effect of curcumin, when loaded into brain-penetrating PLGA-PEG nanoparticles, in the treatment of neonatal brain injury.

## 5 Conclusion

One critical yet underserved population in terms of the development of therapeutic methods is the

neonatal population, for whom PA and subsequent development of HIE are leading causes of death. We sought to evaluate the efficacy of curcumin (a pharmaceutical agent that works on multiple pathways to reduce inflammation and promote neuronal recovery) in a rat model of neonatal brain injury. Therapeutic delivery mediated by the PLGA-PEG polymeric nanoparticle platform was implemented to improve efficacy by increasing drug solubility, stability, bioavailability, and targeting of sites of injury. We show that BBB impairment enhances nanoparticle extravasation into the brain parenchyma, and that a dense PEG coating on the PLGA nanoparticles allows for effective penetration within the brain parenchyma. As a result, when administered systemically, PLGA-PEG/curcumin nanoparticles significantly reduce global injury, but their neuroprotective effect may be most pronounced in the penumbral region, or in less severely injured animals. The neuroprotective effect of curcumin-loaded nanoparticles provides an additional intervention for further research on the treatment of neonatal brain injury.

## Acknowledgements

This manuscript was supported by the Burroughs Wellcome Fund Career Award at Scientific Interfaces (E. N.) and the University of Washington Department of Pediatrics Neonatal Biology Research Grant (P. P.). The content is solely the responsibility of the authors and does not necessarily represent the official views of the Burroughs Wellcome Fund.

**Electronic Supplementary Material:** Supplementary material (Table S1 and Figs. S1–S3) is available in the online version of this article at <https://doi.org/10.1007/s12274-018-2104-y>.

## References

- [1] Parikh, P.; Juul, S. E. Neuroprotective strategies in neonatal brain injury. *J. Pediatr.* **2018**, *192*, 22–32.
- [2] Murray, C. J. L.; Lopez, A. D. Global mortality, disability, and the contribution of risk factors: Global burden of disease study. *Lancet* **1997**, *349*, 1436–1442.

- [3] Kurinczuk, J. J.; White-Koning, M.; Badawi, N. Epidemiology of neonatal encephalopathy and hypoxic-ischaemic encephalopathy. *Early Hum. Dev.* **2010**, *86*, 329–338.
- [4] Robertson, C. M. T.; Perlman, M. Follow-up of the term infant after hypoxic-ischemic encephalopathy. *Paediatr. Child Health* **2006**, *11*, 278–282.
- [5] Jacobs, S. E.; Berg, M.; Hunt, R.; Tarnow-Mordi, W. O.; Inder, T. E.; Davis, P. G. Cooling for newborns with hypoxic ischaemic encephalopathy. *Cochrane Database Syst. Rev.* **2013**, CD003311.
- [6] Edwards, A. D.; Brocklehurst, P.; Gunn, A. J.; Halliday, H.; Juszczak, E.; Levene, M.; Strohm, B.; Thoresen, M.; Whitelaw, A.; Azzopardi, D. Neurological outcomes at 18 months of age after moderate hypothermia for perinatal hypoxic ischaemic encephalopathy: Synthesis and meta-analysis of trial data. *BMJ* **2010**, *340*, c363.
- [7] Dingley, J.; Liu, X.; Gill, H.; Smit, E.; Sabir, H.; Tooley, J.; Chakkarapani, E.; Windsor, D.; Thoresen, M. The feasibility of using a portable xenon delivery device to permit earlier xenon ventilation with therapeutic cooling of neonates during ambulance retrieval. *Anesth. Analg.* **2015**, *120*, 1331–1336.
- [8] Juul, S. E.; Comstock, B. A.; Heagerty, P. J.; Mayock, D. E.; Goodman, A. M.; Hauge, S.; Gonzalez, F.; Wu, Y. W. High-dose erythropoietin for asphyxia and encephalopathy (HEAL): A randomized controlled trial—Background, aims, and study protocol. *Neonatology* **2018**, *113*, 331–338.
- [9] Pauliah, S. S.; Shankaran, S.; Wade, A.; Cady, E. B.; Thayyil, S. Therapeutic hypothermia for neonatal encephalopathy in low- and middle-income countries: A systematic review and meta-analysis. *PLoS One* **2013**, *8*, e58834.
- [10] Zhang, Z. Y.; Jiang, M.; Fang, J.; Yang, M. F.; Zhang, S.; Yin, Y. X.; Li, D. W.; Mao, L. L.; Fu, X. Y.; Hou, Y. J. et al. Enhanced therapeutic potential of nano-curcumin against subarachnoid hemorrhage-induced blood-brain barrier disruption through inhibition of inflammatory response and oxidative stress. *Mol. Neurobiol.* **2017**, *54*, 1–14.
- [11] Wu, A.; Noble, E. E.; Tyagi, E.; Ying, Z.; Zhuang, Y. M.; Gomez-Pinilla, F. Curcumin boosts DHA in the brain: Implications for the prevention of anxiety disorders. *Biochim. Biophys. Acta* **2015**, *1852*, 951–961.
- [12] Ishrat, T.; Hoda, M. N.; Khan, M. B.; Yousuf, S.; Ahmad, M.; Khan, M. M.; Ahmad, A.; Islam, F. Amelioration of cognitive deficits and neurodegeneration by curcumin in rat model of sporadic dementia of Alzheimer's type (SDAT). *Eur. Neuropsychopharmacol.* **2009**, *19*, 636–647.
- [13] Pulido-Moran, M.; Moreno-Fernandez, J.; Ramirez-Tortosa, C.; Ramirez-Tortosa, M. Curcumin and health. *Molecules* **2016**, *21*, 264.
- [14] Sharma, R. A.; Steward, W. P.; Gescher, A. J. Pharmacokinetics and pharmacodynamics of curcumin. In *The Molecular Targets and Therapeutic Uses of Curcumin in Health and Disease. Advances in Experimental Medicine and Biology*; Aggarwal, B. B.; Surh, Y. J.; Shishodia, S., Eds.; Springer: Boston, MA, USA, 2007; Vol. 595, pp 453–454.
- [15] Patel, T.; Zhou, J. B.; Piepmeier, J. M.; Saltzman, W. M. Polymeric nanoparticles for drug delivery to the central nervous system. *Adv. Drug Deliv. Rev.* **2012**, *64*, 701–705.
- [16] Kreuter, J. Nanoparticulate systems for brain delivery of drugs. *Adv. Drug Deliv. Rev.* **2001**, *47*, 65–81.
- [17] Gelperina, S.; Maksimenko, O.; Khalansky, A.; Vanchugova, L.; Shipulo, E.; Abbasova, K.; Berdiev, R.; Wohlfart, S.; Chepurnova, N.; Kreuter, J. Drug delivery to the brain using surfactant-coated poly(lactide-co-glycolide) nanoparticles: Influence of the formulation parameters. *Eur. J. Pharm. Biopharm.* **2010**, *74*, 157–163.
- [18] Huang, N.; Lu, S.; Liu, X. G.; Zhu, J.; Wang, Y. J.; Liu, R. T. PLGA nanoparticles modified with a BBB-penetrating peptide co-delivering A $\beta$  generation inhibitor and curcumin attenuate memory deficits and neuropathology in Alzheimer's disease mice. *Oncotarget* **2017**, *8*, 81001–81013.
- [19] Sathya, S.; Shanmuganathan, B.; Saranya, S.; Vaidevi, S.; Ruckmani, K.; Devi, K. P. Phytol-loaded PLGA nanoparticle as a modulator of Alzheimer's toxic A $\beta$  peptide aggregation and fibrillation associated with impaired neuronal cell function. *Artif. Cells Nanomed. Biotechnol.*, in press, DOI: 10.1080/21691401.2017.1391822.
- [20] Sánchez-López, E.; Egea, M. A.; Davis, B. M.; Guo, L.; Espina M.; Silva, A. M.; Calpena, A. C.; Souto, E. M. B.; Ravindran, N.; Ettcheto, M. et al. Memantine-loaded PEGylated biodegradable nanoparticles for the treatment of glaucoma. *Small* **2018**, *14*, 1701808.
- [21] Ruozi, B.; Belletti, D.; Sharma, H. S.; Sharma, A.; Muresanu, D. F.; Mössler, H.; Forni, F.; Vandelli, M. A.; Tosi, G. PLGA nanoparticles loaded cerebrolysin: Studies on their preparation and investigation of the effect of storage and serum stability with reference to traumatic brain injury. *Mol. Neurobiol.* **2015**, *52*, 899–912.
- [22] Dende, C.; Meena, J.; Nagarajan, P.; Nagaraj, V. A.; Panda, A. K.; Padmanaban, G. Nanocurcumin is superior to native curcumin in preventing degenerative changes in experimental cerebral malaria. *Sci. Rep.* **2017**, *7*, 10062.
- [23] Langert, K. A.; Goshu, B.; Stubbs, E. B., Jr. Attenuation of experimental autoimmune neuritis with locally administered lovastatin-encapsulating poly(lactic-co-glycolic) acid nanoparticles. *J. Neurochem.* **2017**, *140*, 334–346.
- [24] Tang, J.; Li, J. M.; Li, G.; Zhang, H. T.; Wang, L.; Li, D.; Ding, J. S. Spermidine-mediated poly(lactic-co-glycolic acid) nanoparticles containing fluorofenidone for the treatment of idiopathic pulmonary fibrosis. *Int. J. Nanomedicine* **2017**,

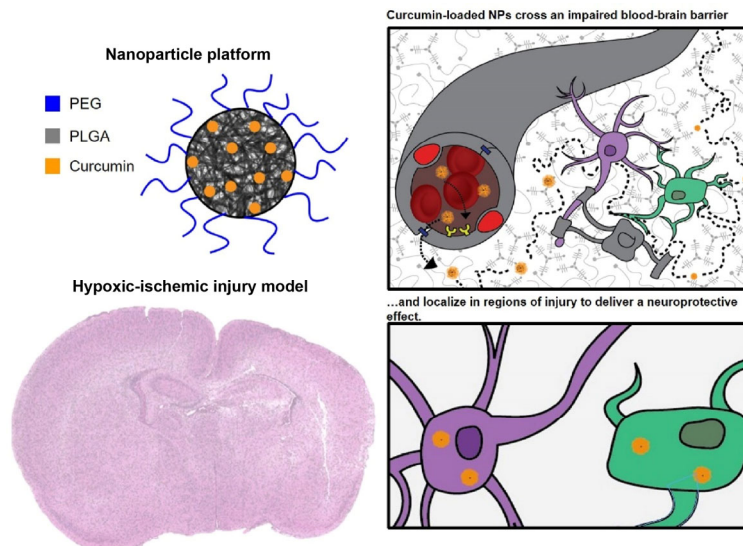
- 12, 6687–6704.
- [25] Cai, Q.; Wang, L.; Deng, G.; Liu, J. H.; Chen, Q. X.; Chen, Z. B. Systemic delivery to central nervous system by engineered PLGA nanoparticles. *Am. J. Transl. Res.* **2016**, *8*, 749–764.
- [26] Nance, E. A.; Woodworth, G. F.; Sailor, K. A.; Shih, T. Y.; Xu, Q. G.; Swaminathan, G.; Xiang, D.; Eberhart, C.; Hanes, J. A dense poly(ethylene glycol) coating improves penetration of large polymeric nanoparticles within brain tissue. *Sci. Transl. Med.* **2012**, *4*, 149ra119.
- [27] Suk, J. S.; Xu, Q. G.; Kim, N.; Hanes, J.; Ensign, L. M. PEGylation as a strategy for improving nanoparticle-based drug and gene delivery. *Adv. Drug Deliv. Rev.* **2016**, *99*, 28–51.
- [28] Mehvar, R. Modulation of the pharmacokinetics and pharmacodynamics of proteins by polyethylene glycol conjugation. *J. Pharm. Pharm. Sci.* **2000**, *3*, 125–136.
- [29] Gref, R.; Minamitake, Y.; Peracchia, M.; Trubetskoy, V.; Torchilin, V.; Langer, R. Biodegradable long-circulating polymeric nanospheres. *Science* **1994**, *263*, 1600–1603.
- [30] Yallapu, M. M.; Nagesh, P. K. B.; Jaggi, M.; Chauhan, S. C. Therapeutic applications of curcumin nanoformulations. *AAPS J.* **2015**, *17*, 1341–1356.
- [31] Mathew, A.; Fukuda, T.; Nagaoka, Y.; Hasumura, T.; Morimoto, H.; Yoshida, Y.; Maekawa, T.; Venugopal, K.; Kumar, D. S. Curcumin loaded-PLGA nanoparticles conjugated with Tet-1 peptide for potential use in Alzheimer's disease. *PLoS One* **2012**, *7*, e32616.
- [32] Ray, B.; Bisht, S.; Maitra, A.; Maitra, A.; Lahiri, D. K. Neuroprotective and neurorescue effects of a novel polymeric nanoparticle formulation of curcumin (NanoCurc) in the neuronal cell culture and animal model: Implications for Alzheimer's disease. *J. Alzheimers Dis.* **2011**, *23*, 61–77.
- [33] Ahmad, N.; Ahmad, I.; Umar, S.; Iqbal, Z.; Samim, M.; Ahmad, F. J. PNIPAM nanoparticles for targeted and enhanced nose-to-brain delivery of curcuminoids: UPLC/ESI-Q-ToF-MS/MS-based pharmacokinetics and pharmacodynamic evaluation in cerebral ischemia model. *Drug Deliv.* **2016**, *23*, 2095–2114.
- [34] Orunoğlu, M.; Kaffashi, A.; Pehlivan, S. B.; Şahin, S.; Söylemezoğlu, F.; Oğuz, K. K.; Mut, M. Effects of curcumin-loaded PLGA nanoparticles on the RG2 rat glioma model. *Mater. Sci. Eng. C* **2017**, *78*, 32–38.
- [35] Zhang, X. M.; Li, X. J.; Hua, H. C.; Wang, A. P.; Liu, W. H.; Li, Y. X.; Fu, F. H.; Shi, Y.; Sun, K. Cyclic hexapeptide-conjugated nanoparticles enhance curcumin delivery to glioma tumor cells and tissue. *Int. J. Nanomedicine* **2017**, *12*, 5717–5732.
- [36] Huang, H. C.; Xu, K.; Jiang, Z. F. Curcumin-mediated neuroprotection against amyloid- $\beta$ -induced mitochondrial dysfunction involves the inhibition of GSK-3 $\beta$ . *J. Alzheimers Dis.* **2012**, *32*, 981–996.
- [37] McDonald, J. W.; Johnston, M. V. Physiological and pathophysiological roles of excitatory amino acids during central nervous system development. *Brain Res. Rev.* **1990**, *15*, 41–70.
- [38] Kole, A. J.; Annis, R. P.; Deshmukh, M. Mature neurons: Equipped for survival. *Cell Death Dis.* **2013**, *4*, e689.
- [39] Xu, Q. G.; Boylan, N. J.; Cai, S. T.; Miao, B. L.; Patel, H.; Hanes, J. Scalable method to produce biodegradable nanoparticles that rapidly penetrate human mucus. *J. Control. Release* **2013**, *170*, 279–286.
- [40] Natarajan, R.; Northrop, N.; Yamamoto, B. Fluorescein isothiocyanate (FITC)-dextran extravasation as a measure of blood-brain barrier permeability. *Curr. Protoc. Neurosci.* **2017**, *79*, 9.58.1–9.58.15.
- [41] Kellert, B. A.; McPherson, R. J.; Juul, S. E. A comparison of high-dose recombinant erythropoietin treatment regimens in brain-injured neonatal rats. *Pediatr. Res.* **2007**, *61*, 451–455.
- [42] Zhang, F.; Nance, E.; Alnasser, Y.; Kannan, R.; Kannan, S. Microglial migration and interactions with dendrimer nanoparticles are altered in the presence of neuroinflammation. *J. Neuroinflammation* **2016**, *13*, 65.
- [43] Nance, E.; Timbie, K.; Miller, G. W.; Song, J.; Louttit, C.; Klibanov, A. L.; Shih, T.-Y.; Swaminathan, G.; Tamargo, R. J.; Woodworth, G. F. et al. Non-invasive delivery of stealth, brain-penetrating nanoparticles across the blood-brain barrier using MRI-guided focused ultrasound. *J. Control. Release* **2014**, *189*, 123–132.
- [44] Nance, E.; Zhang, C.; Shih, T.-Y.; Xu, Q. G.; Schuster, B. S.; Hanes, J. Brain-penetrating nanoparticles improve paclitaxel efficacy in malignant glioma following local administration. *ACS Nano* **2014**, *8*, 10655–10664.
- [45] Nance, E.; Porambo, M.; Zhang, F.; Mishra, M. K.; Buelow, M.; Getzenberg, R.; Johnston, M.; Kannan, R. M.; Fatemi, A.; Kannan, S. Systemic dendrimer-drug treatment of ischemia-induced neonatal white matter injury. *J. Control. Release* **2015**, *214*, 112–120.
- [46] Nance, E.; Zhang, F.; Mishra, M. K.; Zhang, Z.; Kambhampati, S. P.; Kannan, R. M.; Kannan, S. Nanoscale effects in dendrimer-mediated targeting of neuroinflammation. *Biomaterials* **2016**, *101*, 96–107.
- [47] Juul, S. E.; Beyer, R. P.; Bammler, T. K.; McPherson, R. J.; Wilkerson, J.; Farin, F. M. Microarray analysis of high-dose recombinant erythropoietin treatment of unilateral brain injury in neonatal mouse hippocampus. *Pediatr. Res.* **2009**, *65*, 485–492.
- [48] Sabir, H.; Scull-Brown, E.; Liu, X.; Thoresen, M. Immediate hypothermia is not neuroprotective after severe hypoxia-

- ischemia and is deleterious when delayed by 12 hours in neonatal rats. *Stroke* **2012**, *43*, 3364–33670.
- [49] Thoresen, M.; Bågenholm, R.; Løberg, E. M.; Apricena, F.; Kjellmer, I. Posthypoxic cooling of neonatal rats provides protection against brain injury. *Arch. Dis. Child. Fetal Neonatal Ed.* **1996**, *74*, F3–F9.
- [50] Thoresen, M.; Bågenholm, R.; Løberg, E. M.; Apricena, F. The stress of being restrained reduces brain damage after a hypoxic-ischaemic insult in the 7-day-old rat. *Neuroreport* **1996**, *7*, 481–484.
- [51] Pin, T. W.; Eldridge, B.; Galea, M. P. A review of developmental outcomes of term infants with post-asphyxia neonatal encephalopathy. *Eur. J. Paediatr. Neurol.* **2009**, *13*, 224–234.
- [52] Traudt, C. M.; McPherson, R. J.; Bauer, L. A.; Richards, T. L.; Burbacher, T. M.; McAdams, R. M.; Juul, S. E. Concurrent erythropoietin and hypothermia treatment improve outcomes in a term nonhuman primate model of perinatal asphyxia. *Dev. Neurosci.* **2013**, *35*, 491–503.
- [53] Luo, J.; Borgens, R.; Shi, R. Y. Polyethylene glycol immediately repairs neuronal membranes and inhibits free radical production after acute spinal cord injury. *J. Neurochem.* **2002**, *83*, 471–480.
- [54] Wood, T.; Osredkar, D.; Puchades, M.; Maes, E.; Falck, M.; Flatebø, T.; Walløe, L.; Sabir, H.; Thoresen, M. Treatment temperature and insult severity influence the neuroprotective effects of therapeutic hypothermia. *Sci. Rep.* **2016**, *6*, 23430.
- [55] Vannucci, R. C.; Towfighi, J.; Heitjan, D. F.; Brucklacher, R. M. Carbon dioxide protects the perinatal brain from hypoxic-ischemic damage: An experimental study in the immature rat. *Pediatrics* **1995**, *95*, 868–874.
- [56] Sabir, H.; Osredkar, D.; Maes, E.; Wood, T.; Thoresen, M. Xenon combined with therapeutic hypothermia is not neuroprotective after severe hypoxia-ischemia in neonatal rats. *PLoS One* **2016**, *11*, e0156759.
- [57] Towfighi, J.; Mauger, D.; Vannucci, R. C.; Vannucci, S. J. Influence of age on the cerebral lesions in an immature rat model of cerebral hypoxia-ischemia: A light microscopic study. *Dev. Brain Res.* **1997**, *100*, 149–160.
- [58] Wang, Y.; Li, S.-Y.; Shen, S.; Wang, J. Protecting neurons from cerebral ischemia/reperfusion injury via nanoparticle-mediated delivery of an siRNA to inhibit microglial neurotoxicity. *Biomaterials* **2018**, *161*, 95–105.
- [59] Ishii, T.; Fukuta, T.; Agato, Y.; Oyama, D.; Yasuda, N.; Shimizu, K.; Kawaguchi, A. T.; Asai, T.; Oku, N. Nanoparticles accumulate in ischemic core and penumbra region even when cerebral perfusion is reduced. *Biochem. Biophys. Res. Commun.* **2013**, *430*, 1201–1205.
- [60] Ambruosi, A.; Gelperina, S.; Khalansky, A.; Tanski, S.; Theisen, A.; Kreuter, J. Influence of surfactants, polymer and doxorubicin loading on the anti-tumour effect of poly(butyl cyanoacrylate) nanoparticles in a rat glioma model. *J. Microencapsul.* **2006**, *23*, 582–592.
- [61] Ambruosi, A.; Khalansky, A. S.; Yamamoto, H.; Gelperina, S. E.; Begley, D. J.; Kreuter, J. Biodistribution of polysorbate 80-coated doxorubicin-loaded [<sup>14</sup>C]-poly(butyl cyanoacrylate) nanoparticles after intravenous administration to glioblastoma-bearing rats. *J. Drug Target.* **2006**, *14*, 97–105.
- [62] Kulkarni, S. A.; Feng, S. S. Effects of surface modification on delivery efficiency of biodegradable nanoparticles across the blood-brain barrier. *Nanomedicine* **2011**, *6*, 377–394.
- [63] Na, J. H.; Koo, H.; Lee, S.; Min, K. H.; Park, K.; Yoo, H.; Lee, S. H.; Park, J. H.; Kwon, I. C.; Jeong, S. et al. Real-time and non-invasive optical imaging of tumor-targeting glycol chitosan nanoparticles in various tumor models. *Biomaterials* **2011**, *32*, 5252–5261.
- [64] Gref, R.; Lück, M.; Quellec, P.; Marchand, M.; Dellacherie, E.; Harnisch, S.; Blunk, T.; Müller, R.H. “Stealth” corona-core nanoparticles surface modified by polyethylene glycol (PEG): Influences of the corona (PEG chain length and surface density) and of the core composition on phagocytic uptake and plasma protein adsorption. *Colloids Surf. B: Biointerfaces* **2000**, *18*, 301–313.
- [65] Stolnik, S.; Dunn, S. E.; Garnett, M. C.; Davies, M. C.; Coombes, A. G. A.; Taylor, D. C.; Irving, M. P.; Purkiss, S. C.; Tadros, T. F.; Davis, S. S. et al. Surface modification of poly(lactide-co-glycolide) nanospheres by biodegradable poly(lactide)-poly(ethylene glycol) copolymers. *Pharm. Res.* **1994**, *11*, 1800–1808.
- [66] Langer, R. W. Drug delivery and targeting. *Nature* **1998**, *392*, 5–10.
- [67] Zhang, C.; Nance, E. A.; Mastorakos, P.; Chisholm, J.; Berry, S.; Eberhart, C.; Tyler, B.; Brem, H.; Suk, J. S.; Hanes, J. Convection enhanced delivery of cisplatin-loaded brain penetrating nanoparticles cures malignant glioma in rats. *J. Control. Release* **2017**, *263*, 112–119.
- [68] Xiao, R. Z.; Zeng, Z. W.; Zhou, G. L.; Wang, J. J.; Li, F. Z.; Wang, A. M. Recent advances in PEG-PLA block copolymer nanoparticles. *Int. J. Nanomedicine* **2010**, *5*, 1057–1065.
- [69] Allison, S. D. Analysis of initial burst in PLGA microparticles. *Expert Opin. Drug Deliv.* **2008**, *5*, 615–628.
- [70] Yang, C. H.; Zhang, X. J.; Fan, H. G.; Liu, Y. Curcumin upregulates transcription factor Nrf2, HO-1 expression and protects rat brains against focal ischemia. *Brain Res.* **2009**, *1282*, 133–141.
- [71] Esatbeyoglu, T.; Huebbe, P.; Ernst, I. M. A.; Chin, D.; Wagner, A. E.; Rimbach, G. Curcumin—from molecule to biological function. *Angew. Chem., Int. Ed.* **2012**, *51*, 5308–5332.

- [72] Lin, J. K. Molecular targets of curcumin. In *The Molecular Targets and Therapeutic Uses of Curcumin in Health and Disease. Advances in Experimental Medicine and Biology*; Aggarwal, B. B.; Surh, Y. J.; Shishodia, S., Eds.; Springer: Boston, MA, USA, 2007; Vol. 595, pp 227–243.
- [73] Zhu, H. T.; Bian, C.; Yuan, J. C.; Chu, W. H.; Xiang, X.; Chen, F.; Wang, C. S.; Feng, H.; Lin, J. K. Curcumin attenuates acute inflammatory injury by inhibiting the TLR4/MyD88/NF- $\kappa$ B signaling pathway in experimental traumatic brain injury. *J. Neuroinflammation* **2014**, *11*, 59.
- [74] Liu, Z. J.; Liu, W.; Liu, L.; Xiao, C.; Wang, Y.; Jiao, J. S. Curcumin protects neuron against cerebral ischemia-induced inflammation through improving PPAR-Gamma function. *Evid. Based Complement. Alternat. Med.* **2013**, *2013*, 470975.
- [75] Huang, H. C.; Chang, P.; Lu, S.-Y.; Zheng, B.-W.; Jiang, Z.-F. Protection of curcumin against amyloid- $\beta$ -induced cell damage and death involves the prevention from NMDA receptor-mediated intracellular  $\text{Ca}^{2+}$  elevation. *J. Recept. Signal Transduct.* **2015**, *35*, 450–457.
- [76] Tiwari, S. K.; Agarwal, S.; Seth, B.; Yadav, A.; Nair, S.; Bhatnagar, P.; Karmakar, M.; Kumari, M.; Chauhan, L. K. S.; Patel, D. K. et al. Curcumin-loaded nanoparticles potently induce adult neurogenesis and reverse cognitive deficits in Alzheimer's disease model via canonical Wnt/ $\beta$ -catenin pathway. *ACS Nano* **2014**, *8*, 76–103.
- [77] Hagberg, H.; Gressens, P.; Mallard, C. Inflammation during fetal and neonatal life: Implications for neurologic and neuropsychiatric disease in children and adults. *Ann. Neurol.* **2012**, *71*, 444–457.
- [78] Vargas, D. L.; Nascimbene, C.; Krishnan, C.; Zimmerman, A. W.; Pardo, C. A. Neuroglial activation and neuroinflammation in the brain of patients with autism. *Ann. Neurol.* **2005**, *57*, 67–81.
- [79] O'Callaghan, J. P.; Sriram, K.; Miller, D. B. Defining "neuroinflammation". *Ann. N. Y. Acad. Sci.* **2008**, *1139*, 318–330.
- [80] Hassell, K. J.; Ezzati, M.; Alonso-Alconada, D.; Hausenloy, D. J.; Robertson, N. J. New horizons for newborn brain protection: Enhancing endogenous neuroprotection. *Arch. Dis. Child. Fetal Neonatal Ed.* **2015**, *100*, F541–F552.
- [81] Ameruoso, A.; Palomba, R.; Palange, A. L.; Cervadoro, A.; Lee, A.; Di Mascolo, D.; Decuzzi, P. Ameliorating amyloid- $\beta$  fibrils triggered inflammation via curcumin-loaded polymeric nanoconstructs. *Front. Immunol.* **2017**, *8*, 1411.
- [82] Umerska, A.; Gaucher, C.; Oyarzun-Ampuero, F.; Fries-Raeth, I.; Colin, F.; Villamizar-Sarmiento, M. G.; Maincent, P.; Sapin-Minet, A. Polymeric nanoparticles for increasing oral bioavailability of curcumin. *Antioxidants* **2018**, *7*, 46.
- [83] Verderio, P.; Bonetti, P.; Colombo, M.; Pandolfi, L.; Prosperi, D. Intracellular drug release from curcumin-loaded PLGA nanoparticles induces G2/M block in breast cancer cells. *Biomacromolecules* **2013**, *14*, 672–682.
- [84] Basniwal, R. K.; Khosla, R.; Jain, N. Improving the anticancer activity of curcumin using nanocurcumin dispersion in water. *Nutr. Cancer* **2014**, *66*, 1015–1022.
- [85] Berger, H. R.; Morken, T. S.; Vettukattil, R.; Brubakk, A.-M.; Sonnewald, U.; Widerøe, M. No improvement of neuronal metabolism in the reperfusion phase with melatonin treatment after hypoxic-ischemic brain injury in the neonatal rat. *J. Neurochem.* **2016**, *136*, 339–350.
- [86] Di Giorgio, A. M.; Hou, Y. J.; Zhao, X. R.; Zhang, B.; Lyeth, B. G.; Russell, M. J. Dimethyl sulfoxide provides neuroprotection in a traumatic brain injury model. *Restor. Neurol. Neurosci.* **2008**, *26*, 501–507.
- [87] Smith, A. L.; Garbus, H.; Rosenkrantz, T. S.; Fitch, R. H. Sex differences in behavioral outcomes following temperature modulation during induced neonatal hypoxic ischemic injury in rats. *Brain Sci.* **2015**, *5*, 220–240.
- [88] Burns, J. C.; Chavez-Valdez, R.; Hossain, M. S.; Kesavan, K.; Martin, L. J.; Zhang, J. Y.; Northington, F. J. Hypoxia-ischemia and therapeutic hypothermia in the neonatal mouse brain—A longitudinal study. *PLoS One* **2015**, *10*, e0118889.
- [89] Smith, A. L.; Alexander, M.; Rosenkrantz, T. S.; Sadek, M. L.; Fitch, R. H. Sex differences in behavioral outcome following neonatal hypoxia ischemia: Insights from a clinical meta-analysis and a rodent model of induced hypoxic ischemic brain injury. *Exp. Neurol.* **2014**, *254*, 54–67.
- [90] Cohen, S. S.; Stonestreet, B. S. Sex differences in behavioral outcome following neonatal hypoxia ischemia: Insights from a clinical meta-analysis and a rodent model of induced hypoxic ischemic injury. *Exp. Neurol.* **2014**, *256*, 70–73.
- [91] Nie, X. J.; Lowe, D. W.; Rollins, L. G.; Bentzley, J.; Fraser, J. L.; Martin, R.; Singh, I.; Jenkins, D. Sex-specific effects of N-acetylcysteine in neonatal rats treated with hypothermia after severe hypoxia-ischemia. *Neurosci. Res.* **2016**, *108*, 24–33.
- [92] Demarest, T. G.; McCarthy, M. M. Sex differences in mitochondrial (dys)function: Implications for neuroprotection. *J. Bioenerg. Biomembr.* **2015**, *47*, 173–188.
- [93] Jatana, M.; Singh, I.; Singh, A. K.; Jenkins, D. Combination of systemic hypothermia and N-acetylcysteine attenuates hypoxic-ischemic brain injury in neonatal rats. *Pediatr. Res.* **2006**, *59*, 684–689.



## Table of contents



Curcumin-loaded brain-penetrating nanoparticles can cross the impaired blood-brain barrier following systemic administration in a neonatal hypoxia-ischemia rat model. The brain-penetrating nanoparticles localize in regions of injury and release curcumin to provide a neuroprotective effect, expanding the number of clinically-relevant therapeutic interventions for the treatment of neonatal hypoxic-ischemic encephalopathy.



## Electronic Supplementary Material

# Curcumin-loaded polymeric nanoparticles for neuroprotection in neonatal rats with hypoxic-ischemic encephalopathy

Andrea Joseph<sup>1</sup>, Thomas Wood<sup>2</sup>, Chih-Chung Chen<sup>1,†</sup>, Kylie Corry<sup>2</sup>, Jessica M. Snyder<sup>3</sup>, Sandra E. Juul<sup>2</sup>, Pratik Parikh<sup>2</sup>, and Elizabeth Nance<sup>1,4</sup> (✉)

<sup>1</sup> Department of Chemical Engineering, University of Washington, Seattle, WA 98195, USA

<sup>2</sup> Division of Neonatology, Department of Pediatrics, University of Washington, Seattle, WA 98195, USA

<sup>3</sup> Department of Comparative Medicine, University of Washington, Seattle, WA 98195, USA

<sup>4</sup> Department of Radiology, University of Washington, Seattle, WA 98195, USA

<sup>†</sup> Present address: Department of Bioengineering, University of Illinois at Urbana-Champaign, Urbana, Illinois 61801, USA

Supporting information to <https://doi.org/10.1007/s12274-018-2104-y>

**Table S1 Neuropathological scoring criteria.** Region-specific scoring used for evaluation of neuropathology in saline, free curcumin, blank PLGA-PEG, and PLGA-PEG/curcumin treatment groups.

Score	Cortex, Striatum, Thalamus		Hippocampus
	Percent involved	Criteria	
0	Normal		No injury
0.5	<10 necrotic neurons		<10 scattered necrotic neurons
1	<10%	small, patchy	<10%; dentate not involved
1.5	10-20%	patchy	<50% or if dentate is involved
2	21-30%	partly confluent or incomplete	50%; patchy areas necrotic neurons CA1-4
2.5	31-40%	mostly confluent	Coalescing compared to score of 2; <75% affected
3	40-60%	large, confluent, complete	75%; extensive
3.5	61-80%	severe	76-95%
4	>80%	with cystic rarefaction	complete infarction including dentate (100%)

Address correspondence to [eanance@uw.edu](mailto:eanance@uw.edu)

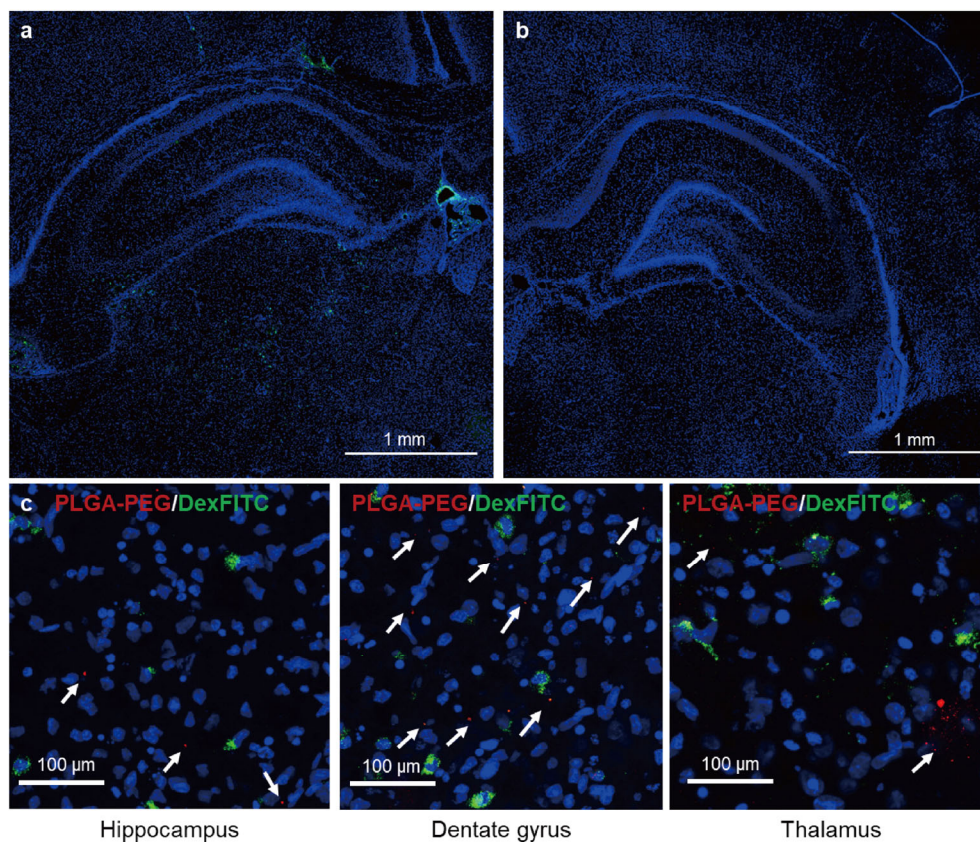


**Figure S1 BBB impairment in HI pups.** 70 kDa Dextran-FITC (7.5g/kg, green) and AF647-labeled PLGA-PEG nanoparticles (50 mg/kg, red) were administered i.p. 30 min after HI in P7 pups. Pups were sacrificed 24 h after HI and perfused. (a) Dextran-FITC extravasation from the impaired blood-brain barrier is observed in the ipsilateral (injured) hemisphere. Scale bar: 1 mm. (b) Limited or no extravasation is observed in the contralateral (uninjured) hemisphere. Scale bar: 1 mm. (c) PLGA-PEG particle extravasation was observed in regions of BBB impairment and dextran-FITC extravasation, including the ipsilateral hippocampus, dentate gyrus, and thalamus. Blue: DAPI cell nuclei stain in all images. Scale bars: 100  $\mu\text{m}$ .

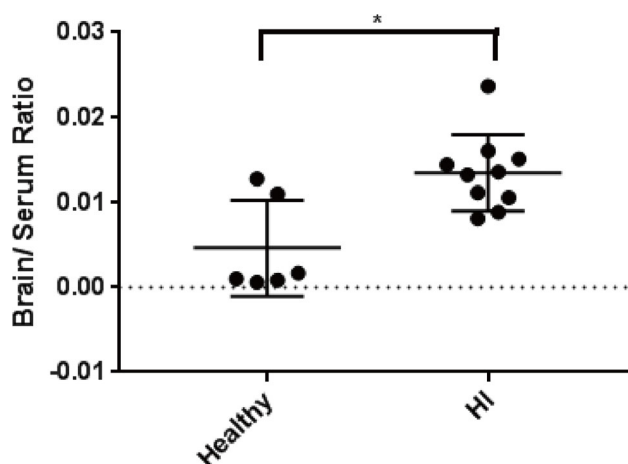


**Figure S2 Biodistribution of AF647-labeled PLGA-PEG nanoparticles 24 hours after injection.** Fluorescently labeled nanoparticles were injected at a 150 mg/kg dose to healthy (n=6, injected at t=0) and HI (n=10, injected 30 min after injury) pups on P7 and pups were perfused and sacrificed after 24 h. Nanoparticle concentration in the brain and serum was measured by UV-Vis and normalized to sample volume or mass. The brain/serum ratio in HI pups (0.0135) was significantly higher (p=0.0037) than the brain/serum ratio in healthy pups (0.0047) indicating enhanced brain penetration of the PLGA-PEG vehicle after hypoxic-ischemic injury.

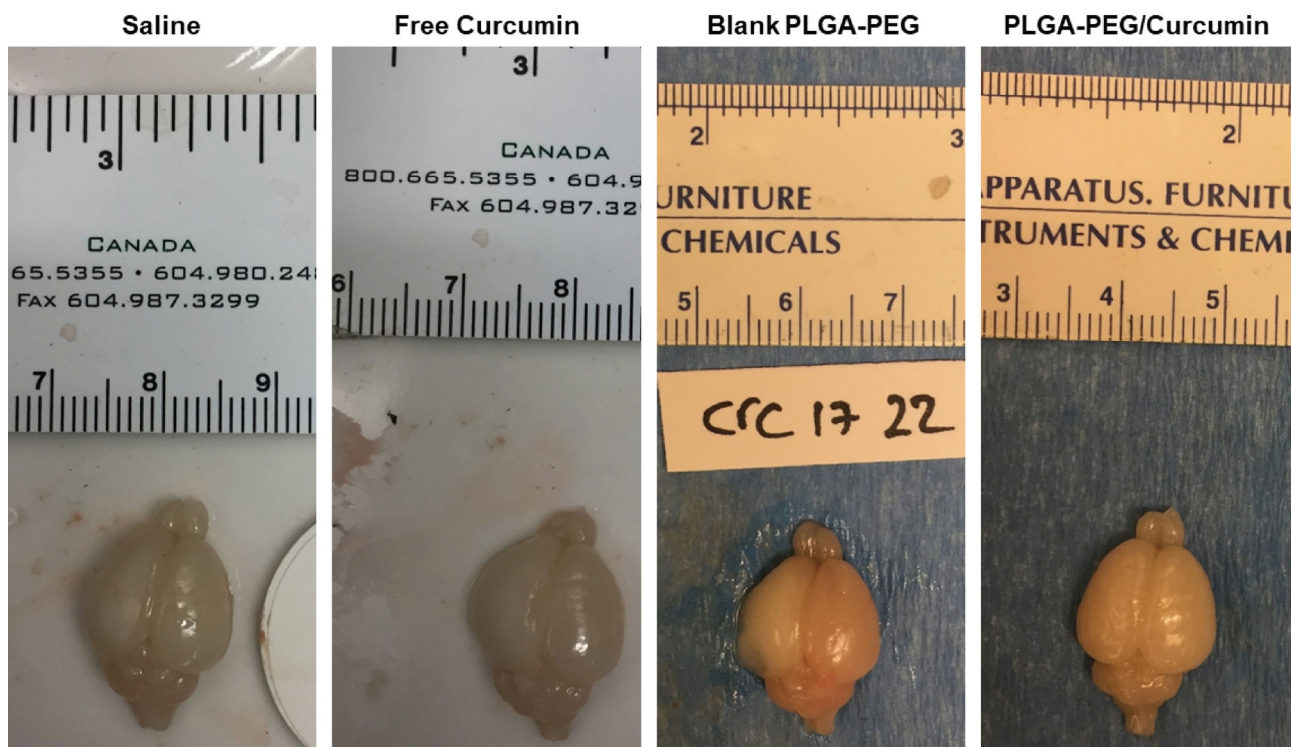


**Figure S3 Representative gross injury in HI pups.** For each treatment group, a representative picture of the median animal used for gross injury scoring is provided.